LOW CURING TEMPERATURE FERROMAGNETIC INK DEVELOPMENT AND APPLICATION IN 3D PRINTED RF ANTENNA DESIGN AND MINIATURIZATION

by

Evarestus C. Enuka

A thesis submitted to the Graduate Council of
Texas State University in partial fulfillment
of the requirements for the degree of
Master of Science
with a Major in Engineering
August 2017

Committee Members:

Yihong Maggi Chen, Chair

Ravi Droopad

Qingkai Yu

FAIR USE AND AUTHOR'S PERMISSION STATEMENT

Fair Use

Duplication Permission

DEDICATION

To the blessed memory of my father: Anthony Enuka

ACKNOWLEDGEMENTS

I sincerely extend my profound gratitude to my advisor Dr. Maggi Yihong Chen for her valuable advice and financial support over the period of this work. My appreciation also goes to other committee members Prof Ravi Droopad and Dr. Qingkai Yu for making out time to read this thesis and for their expert contributions. Special thanks to the graduate advisor Professor Vishu Viswanathan and administrative sectary Sarah Rivas for their administrative assistance.

This thesis would not have been possible without the support and encouragements from my lovely mom Mrs. Roseline Enuka and my siblings Chinedu, Augustine, Cosmas, Martha, Emmanuel, Emelda and Ester. They remain the backbone of my success.

Am also grateful to my friends especially, Assumpta Okoye for being there for me despite all odds, Emmanuel Madu and his family for their support. Mahmuda Monne for her contributions in this work.

I would also like to express my deepest appreciation to the National Aeronautics and Space Administration (NASA) and Nothrop grumen for their financial support.

TABLE OF CONTENTS

Page

LIST OF TABLES

Table **Page**

LIST OF FIGURES

Figure **Page**

ABSTRACT

In recent times, there has been an increasing demand for smaller size electronic and mobile devices because of advances in engineering and nanotechnology. This has pushed further the need for small size RF antenna with light weight and ease of fabrication especially in areas of communication, biomedical, automobiles, aerospace and military applications etc. Effective antenna miniaturization with improved performance remains a bane to achieving reduced size electronic devices. This is largely due to the inevitable tradeoff between the antenna dimension which depends on its electrical wavelength, and performance of the antenna which is tightly bound to the fundamental limits based on its size. New generation mobile devices are required to have multiple antennae in one device to span multiple frequency ranges such as GSM, LTE, WiMAX, WLAN or Wi-Fi, hence miniaturization becomes imperative.

Integrating ferrite materials in antenna structure have been recently identified as a potential means of reducing antenna size and improving its performance. Magneto-dielectric material, which has both permittivity and permeability greater than unity has been used to demonstrate this possibility. Since this idea came to light, the field of antenna miniaturization has witnessed a meteoric rise in research interest among device engineers. The major research focus is in printed electronics.

Printed electronics has revolutionized the electronic component and device industry. Since its introduction into the main stream of electronic manufacturing industry, inkjet printing technique has attracted a lot of interest because of its low cost of

fabrication of integrated circuit, compatibility with various substrate. This technique has been used in fabricating functional electronic components such as organic thin-film transistors, light-emitting diodes, solar cells, conductive structures, memory devices, sensors, and biological/pharmaceutical tasks. Single and multi-layer printing with various thicknesses have also been achieved using inkjet printing without rigorous effort. Despite these abilities, inkjet printing technique is not commonly used in magneto-dielectric substrate fabrication because high quality ferromagnetic ink that yields magneto-dielectric material with good microwave performance is not readily available in commercial mainstream and therefore need to be synthesized using novel approach.

The objective of this thesis is to develop a high quality ferromagnetic ink with good microwave performance suitable for inkjet printing technique and investigation of the microwave performance of 3D inkjet printed antennae using the developed ink. Different characterization methods are used in this work to evaluate the performance and suitability of the developed ferromagnetic ink in inkjet printing technique. Furthermore, the potential for antenna miniaturization is also demonstrated using different measurement data. Several antennae design and configurations on different magneto-dielectric material substrates are discussed, and compared in terms of their performance with other antennae on conventional high dielectric constant material substrate. Both simulation and measurement data shows that an antenna on magneto-dielectric material substrate has better and improved microwave performance compared to an antenna of the same dimension on a conventional high dielectric material substrate.

1. INTRODUCTION

Background

Recent advances in internet of things (IoT) and cloud computing have caused a tremendous increase in the number of smart devices that supports communication in one or more forms, and this as an effect, has significantly changed our living patterns as humans. Similar developments in wireless communication technologies such as cellular communications (3G or LTE,4G) and Wireless Local Area Networks (WLANs), have made it possible for smartphones and other hand held electronic devices to access the internet almost in any part of the world and this have increased the demand for portable and handheld mobile devices. To meet up with the increasing demands in mobile devices, engineers are recently faced with the challenge of developing more robust light weight, small size and low power requirement mobile and hand held devices to support our daily life. Although, a lot of progress have been made in some areas of microelectronics towards achieving a robust system-on-chip (SoC), miniaturization and complete integration of radio frequency (RF) circuit remains a major challenge for device engineers.

The major factor hindering the development of a fully inkjet printed and flexible RF front end is the physical dimension of the antenna unit. The performance of an antenna is primarily determined by its size which depends on its electrical wavelength (Ikonen P. M., 2006). New generation smartphones and other mobile devices usually have more than one antennae to support operation in different frequency ranges, e.g. a typical mobile phone has antennae that supports operations in GSM 850/900MHz or LTE

1700/2100MHz at once and supports GPS and Bluetooth services, thus efficient antenna miniaturization becomes imperative towards achieving robust and light weight devices. The dependency of some antenna key performance parameters on its physical dimension and limitations of small size antennae have been identified and reported in literature, per (Wheeler H. A., 1947) , the antenna size limits efficiency, bandwidth and radiation resistance values. One other limitation of electrically small antenna is the difficulty in correctly feeding the antenna (Staub, O., J-F. Zürcher, and A. Skrivervik., 1998). Therefore, typical antenna design is a compromise between bandwidth, gain, radiation and size. The best compromise is achieved when the entire antenna volume is excited for radiation.

Furthermore, since antenna miniaturization is the current research focus of antenna design and fabrication engineers, it is very important to understand the fundamental limit of small antennae.

Fundamental Limit of Electrically Small Antennas

An antenna is electrically small when its physical dimensions are small compared to the wavelengths of the electromagnetic fields they radiate. More specifically, the term "electrically small antenna" is understood to include any antenna which fits inside a sphere of radius a= l/k where k is the wave number associated with the electromagnetic field (Wheeler H. A., Small antennas, 1975), (Hansen R. C., 1981), (James S. McLean, 1996). Another commonly used definition of electrically small antenna is any antenna that satisfies the condition

$Ka < 0.5$

Where k is the wave number $2\pi/\lambda$, and *a* is the radius of minimum sphere that encloses the antenna. This spherical enclosure is commonly called the *chu sphere*. (Wheeler H. A., 1947) was the first to investigate the radiation power of electrically small antennae inside a sphere. He observed that the reduction of antenna size places a fundamental limitation on the bandwidth. Later (Chu, 1948) showed that for a vertically polarized antenna, based on three criteria for optimum performance:

(1) maximum gain for a given complexity of the antenna structure

(2) minimum quality factor (Q),

(3) maximum ratio gain (G) to quality factor (Q) (G/Q).

It is found that such an antenna of which the maximum dimension is 2a has the potentiality of a

broad bandwidth provided that the gain is equal to or less than $4a/\lambda$. Where λ is the wavelength. He further showed that to obtain a gain higher than this value, the Q of the antenna increases at an astronomical rate and finally conclude that the antenna which has potentially the broadest bandwidth of all omnidirectional antennas is one which has a radiation pattern corresponding to that of an infinitesimally small dipole. (Harrington, 1960) extended this approximate theory to include both circularly polarized antenna. He was the first to consider the antenna as radiating both TE and TM modes. Both Chu and Harrington works are based on equivalent circuit approximations for representing each generated mode. The limits on electrically small antennas according to (Chu, 1948) are derived by assuming that the entire antenna structure (with a largest linear dimension of $2r$), and its transmission line and oscillator are all enclosed within a sphere of radius *r* as shown in Fig 1.

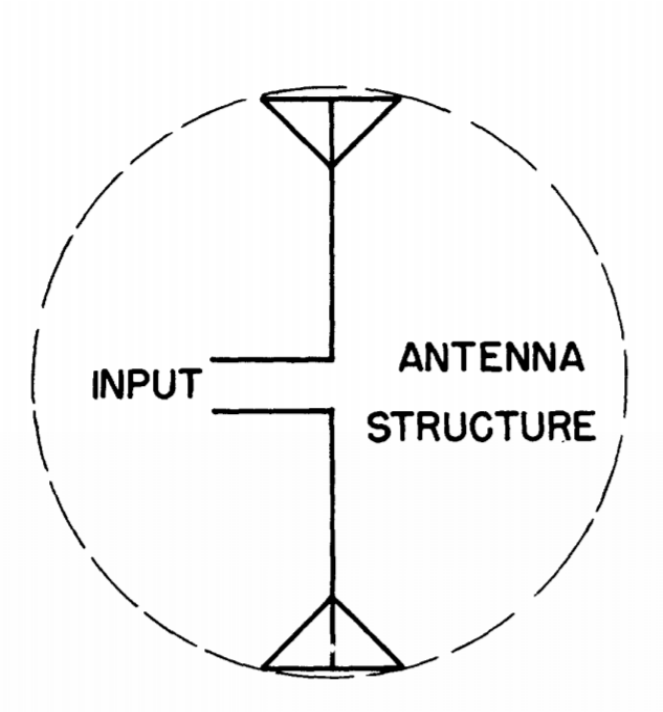

Figure 1. Schematic of a vertically polarized antenna (Chu,1948).

Because of the orthogonal properties of the spherical wave functions employed, the total energy, electric or magnetic, stored outside the sphere is equal to the sum of the corresponding energies associated with each spherical wave, and the complex power transmitted across a closed spherical surface is equal to the sun of the complex

powers associated with each spherical wave.

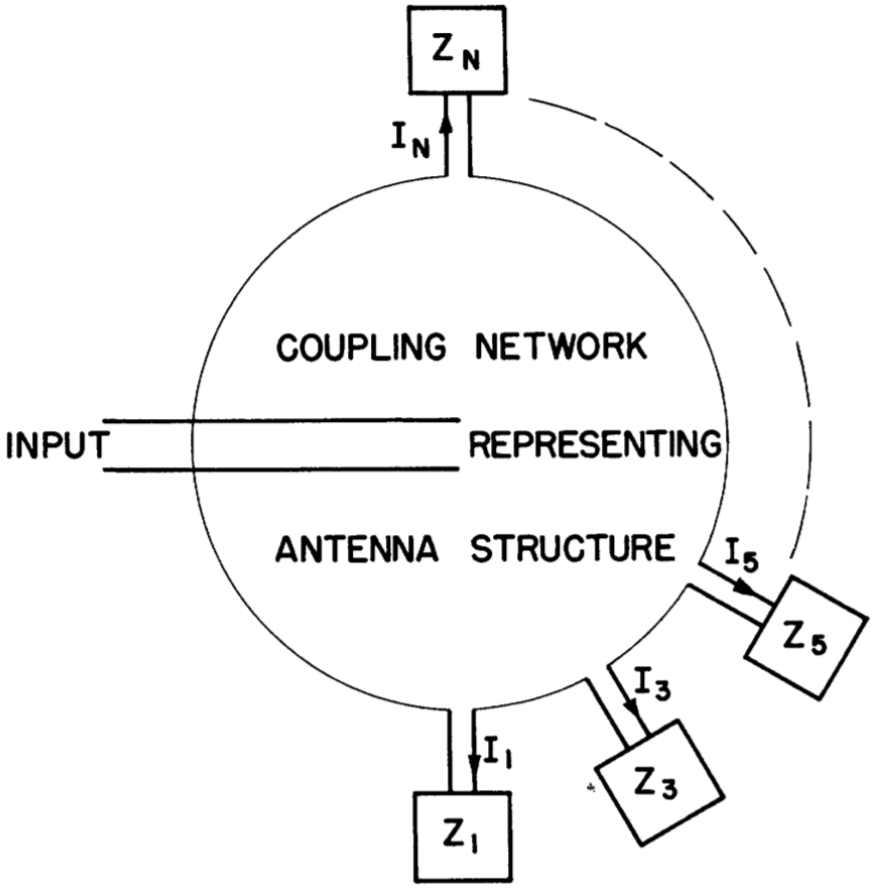

Figure 2: **Equivalent circuit of a vertically polarized omnidirectional antenna (Chu,1948).**

(Balanis, 2005) while explaining the mathematical formulation introduced by Chu, stated that the source or current distribution of the antenna system inside the sphere is not uniquely determined by the field distribution outside the sphere. Since it is possible to determine an infinite number of different source or current distributions inside the sphere, for a given field configuration outside the sphere. Because the spherical wave modes outside the sphere are orthogonal, the total energy (electric or magnetic) outside the sphere and the complex power transmitted across the closed

spherical surface are equal, respectively, to the sum of the energies and complex powers associated with each corresponding spherical mode. Therefore, there is no coupling, in energy or power, between any two modes outside the sphere. As a result, the space outside the sphere can be replaced by several independent equivalent circuits. Figure 2 depicts the equivalent circuit of the field outside the sphere. The Q of an antenna is a very important quantity because it is inversely related to the bandwidth of the antenna. For electrically small antennae enclosed in a sphere, the Q was first studied by (Chu, 1948), it was shown that the TE, TM or TE and TM modes excited in the sphere depends the shape of the radiating element within the bounds of the sphere. Later, (Balanis, 2005) while explaining the mathematical formulation of chu, using the minimum Q plot shown in figure 3, concludes that the bandwidth of an antenna (which can be closed within a sphere of radius r) can be improved only if the antenna utilizes efficiently, with its geometrical configuration, the available volume within the sphere.

However, the works of Wheelar was seen as a rough approximation, while Chu's equivalent circuit approximations was considered inaccurate to establish a fundamental limit of Q. (Thiele G.A., 2003) observed that the theoretical limits on Q according to Wheelar and Chu are far from the actual results obtained for practical antennas. He argued that the current distribution on the antenna had a strong effect on the value of Q. His analysis involved determination of Q from far-filed pattern rather than the usual modal expansion. The results obtained agreed with the current distribution in a practical dipole antenna. The most recent work of (Gustafsson M., 2007) as reported by (Volakis, 2009) provided expressions for Q and gain of

electrically small antennas using scattering theory and representing the antenna in terms of material dyadics. His work indicates the possibility of numerical computations of accurate gain and Q limitations.

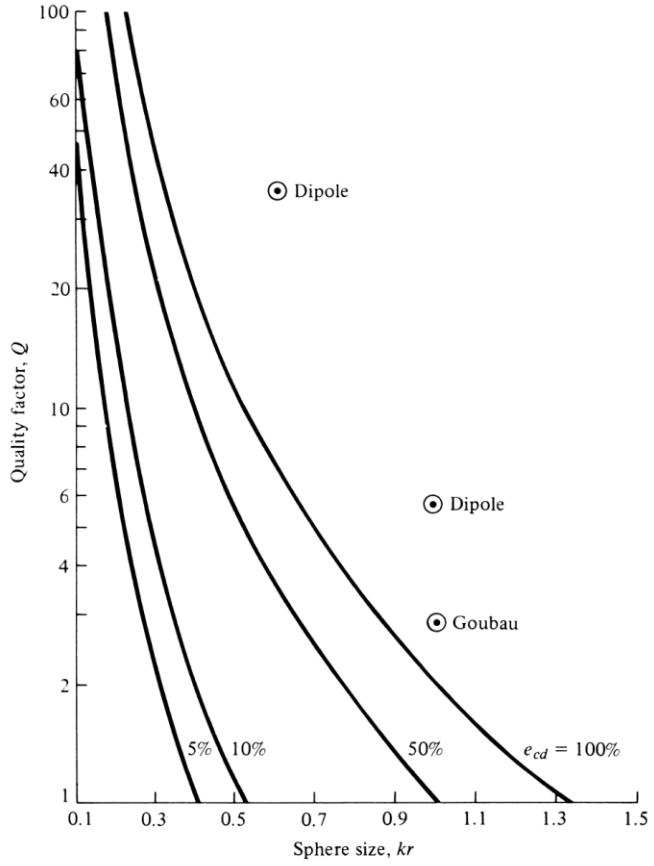

Figure 3: Fundamental limits of *Q* versus antenna size (enclosed within a sphere of radius for single-mode antennas of various radiation efficiencies. (SOURCE: R. C. Hans "Fundamental Limitations in Antennas," *Proc. IEEE*, Vol. 69, No. 2, February 1981. (1981) IEEE)

Table 1: Summary of small antenna Q Limits for Chu Sphere of radius *a* (Volakis, 2009)

Minimum Q	Reference	Notes
$\frac{1}{ka}+\frac{1}{(ka)^3}$	(James S. McLean, 1996)	Assumes TE or TM modes radiation only
$\frac{1}{2}\left(\frac{2}{ka}+\frac{1}{(ka)^3}\right)$	(James S. McLean, 1996)	Assumes TE and TM modes radiation only
$\frac{1.5}{(ka)^3}$	(Thal H.L., 2006)	Assumes a surface current distribution over the Chu sphere surface radiating a TE mode
$\frac{3}{(ka)^3}$	(Thal H.L., 2006)	Assumes a surface current distribution over the Chu sphere surface radiating a TM mode
$\frac{1}{(ka)^3}$	(Thal H.L., 2006)	Assumes a surface current distribution over the Chu sphere surface radiating a TE and TM mode
$\frac{G}{\acute{\eta}}\frac{1}{2(ka)^3}$	(Gustafsson M., 2007)	G = antenna gain ή = antenna absorption efficiency. Assumes antenna composed of PEC material.

Antenna Miniaturization Techniques

It is well established fact that the impedance bandwidth of an antenna is implicitly proportional to the volume of the antenna. The implication is that reducing the size of antenna degrades the impedance bandwidth. However, advances in communication industry is towards light weight, low power requirement and small size devices and therefore, efficient miniaturization of RF front end, particularly the size of antenna becomes imperative.

Antenna miniaturization is a very challenging task which has witnessed a meteoric rise in research interest because of the importance of small antennas in various

applications. Different techniques have been explored in achieving antenna miniaturization and reported in literature. These techniques can be classified into two broad categories, thus:

Miniaturization through geometry modification

Modification of the antenna geometry is the most widely used technique in antenna miniaturization. Geometry modification includes folding, bending, meandering, slot loading, fractal folding spiral shaping etc.

Slot Loading

This is commonly used in miniaturization of planar antennas such as patch antenna. Planar antennas are widely used in communication industry because of its low profile and ease of fabrication. For a standard patch antenna, current flows from one edge of the patch to another, by cutting slot in the metallic patch as shown in figure 4, the current path is increased and thereby reducing the resonance frequency of the antenna.

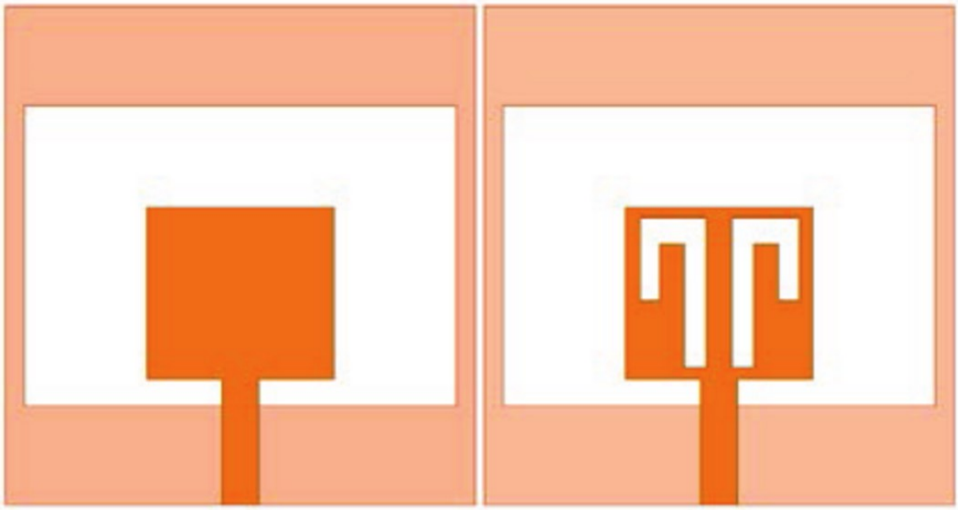

(a) **(b)**

Figure 4: (a) Square patch antenna. (b) square patch antenna with slot loading

Slots of different shapes e.g. square, circular triangular etc. have been used to achieve miniaturization. (Mak, Lai, Luk, & Chan, 2014) recently loaded a circularly polarized patch antenna fabricated on a square PCB with $\varepsilon_r = 2.65$ with 8 slots and this lead to an improved performance with significant size reduction. (Zhou Y. Chen C. C., 2009) designed a proximity fed dual-band stacked patch operating at 1575MHz and 1250MHz for GPS reception. To force meandering of current, slots were cut on the top patch and this lead to reduction of the patch to λ/10, which is equivalent to five fold size reduction from the λ/2 size patch, without degrading the performance of the antenna.

Meander Line Antenna

This is widely used in mobile phones and in network cards in PC and laptops. First versions of this type of antenna was proposed as a winding wire structures by (Rashed J., 1982).

Meander line antennas consist of a continuous periodically folded structure as shown in figure1.5. The current path in a meander line antenna is $2(l + w)$ which obviously shows when compared with a straight monopole of the same length, the meander line antenna will resonate at a lower frequency and therefore reducing the size of the antenna. (Volakis, 2009) compared a conventional dipole of 300mm tall and a resonant frequency of 500MHz with three different configurations of meander line antenna (M1, M2, M3). The meander line antennas resonate at 320, 300, 260 respectively.

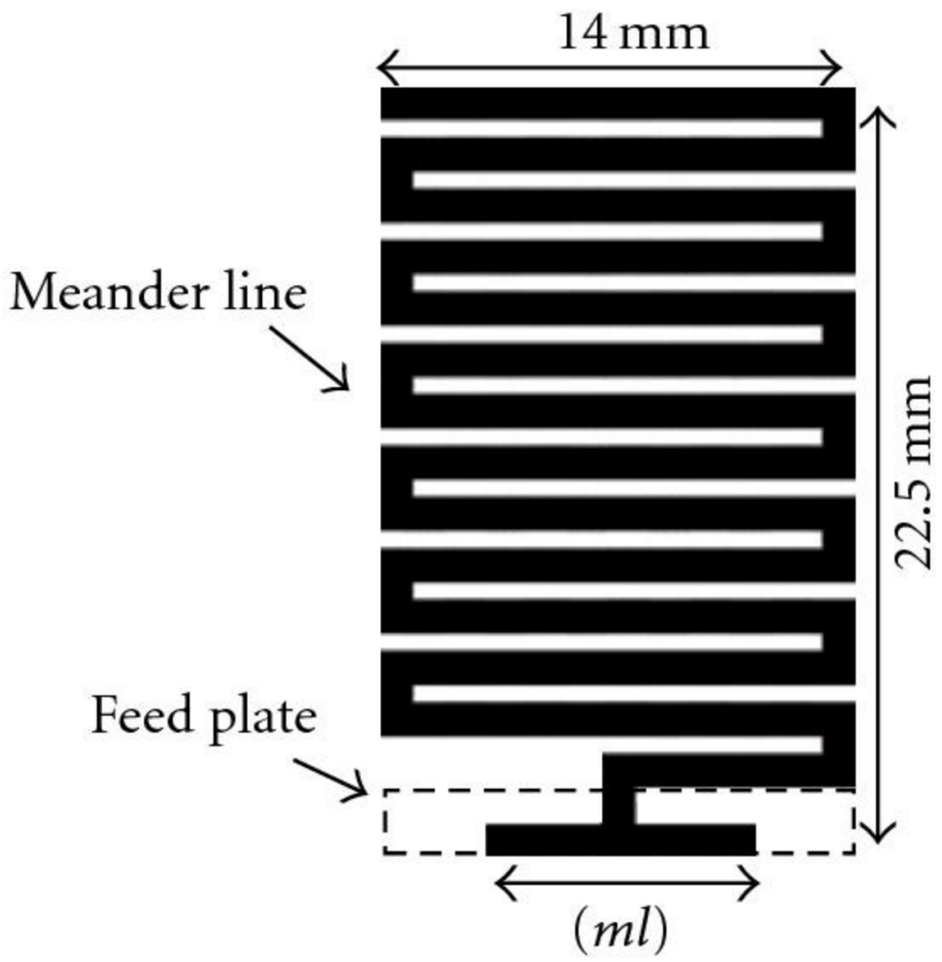

Figure 5: Meander Line antenna

Bending and Folding

Bending and folding have been used to reduce the size of antennas. This kind of geometry modification forces current to flow along a curved and long path resulting in lower resonant frequency (Volakis, 2009). A typical example is the planar inverted-F antenna (PIFA) shown in figure 6. Placing a shorting pin next to the feed on planar inverted-F antenna (PIFA) is another technique for reducing the antenna size, as shown in Figure 6. PIFA is usually a quarter wavelength resonant antenna, however, its size can be reduced further by properly positioning the shorting pin or folding the patch into multiple layers and this configuration is widely adopted in practical wireless devices.

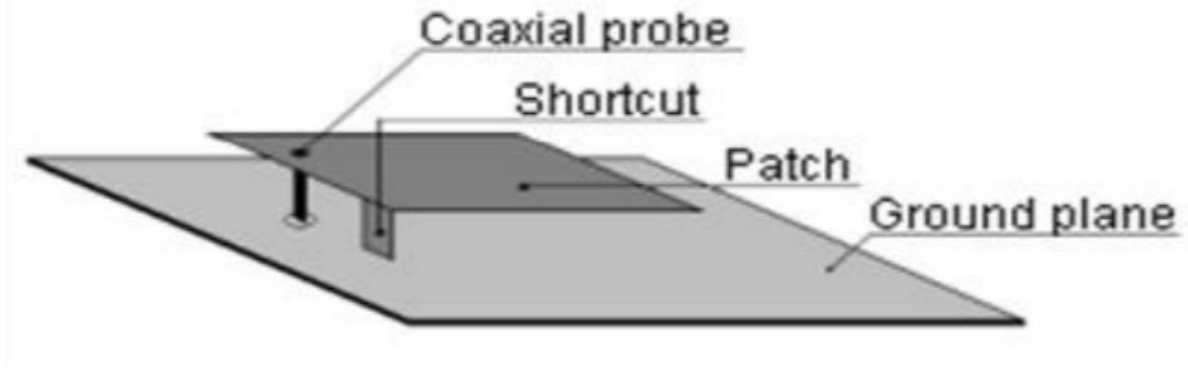

Figure 6: Planar Inverted-F Antenna

PIFA size can further be reduced by capacitive loading of the top plate, this loading compensate for the inductive impedance and hence reducing the size and also the loss of the antenna. Other methods of reducing the size PIFA includes dielectric loading between the ground plane and plate (Hwang Y., 1995), increasing the electrical length by introducing slots (Lo T.K., 2004), optimization of the position of shorting pins (Waterhouse R. B., 1998). Antenna ground plane has a significant effect on the overall size and performance of antenna. As in most mobile phone and network device antennas, it is comparable in size to the radiating element. However, shape can be considered to reduce the antenna size (Huynh M.C., 2004).

Lumped Loading

Lumped elements of capacitor and\or inductors have been effectively used in antenna miniaturization. Different geometry modification technique such as meandering, folding etc. can also be explained using lumped loading concept. (Kramer, Chen, & Volakis, 2008) achieved miniaturization of a spiral antenna on a ferrite coated metal ground plane using both inductive and capacitive loading as shown in figure 7. A realized gain of -15dBi was obtained at 190MHz using the treated spiral compared to untreated spiral on a metallic ground plane which achieved -15dBi gain at 350MHz. Folding

increases capacitance of the antenna element, (Scardelletti, 2008) achieved improved return loss with a reduced resonant frequency of about 22% using a CPW-fed folded slot. However, the use of lumped elements increases loss in the antenna system as well as imposing power handling limitations in the overall system (Lee M. K., 2007) but it is a preferred technique in antenna miniaturization in variety of applications because of its robustness. (Chi, 2011) used a periodic loading of printed high-frequency (HF) slot-loop antenna and a planar inverted F antenna (PIFA) with shunt capacitors figure 8, to exploit the slow wave enhancement factor from loaded transmission line models. It was observed that the enhancement factor agreed with the miniaturization factor. The loaded slot loop presents the predicted gain and measured bandwidth on the order of -34.9 dBi and 0.38% for VSWR ≤ 2, respectively while the measured radiation gain and bandwidth of the loaded PIFA are reduced to -22.6 dBi and 0.15% for VSWR ≤ 2, respectively,

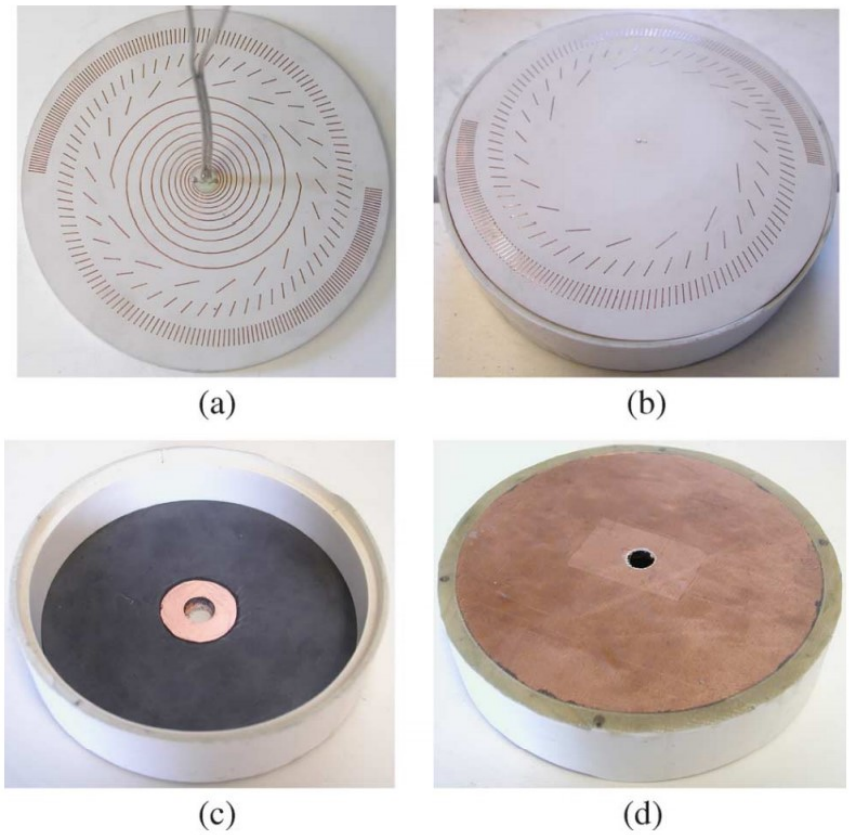

Figure 7: Photos of the fabricated 6 inductively loaded spiral antenna. (a) Bottom side of the inductively loaded spiral PCB. (b) Top side of the complete antenna assembly showing the PVC cavity. (c) View of the PVC cavity showing the ferrite material and copper patch on top of the ferrite. (d) Bottom view of the antenna cavity showing the copper ground plane (Kramer, Chen, & Volakis, 2008).

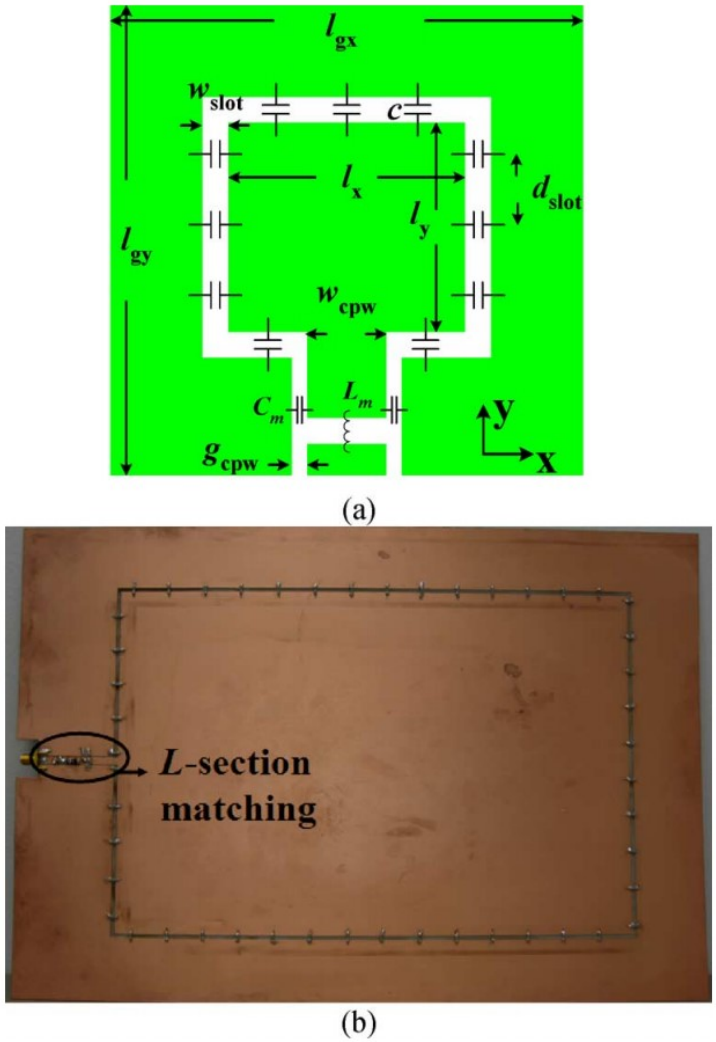

Figure 8: (a) capacitor-loaded HF slot-loop antenna with the -section matching circuit. (b) Photograph of the fabricated antenna.

Miniaturization through material loading

Over the period of last decade, antenna miniaturization by loading the antenna volume at strategic points with high contrast materials has become a widely-used technique and an area of great research interest. It is a general belief that material loading provides a wave slowdown in a manner proportional to $1/\sqrt{\mathcal{E}r\mu r}$ (Volakis, 2009). It also helps in impedance matching because the characteristics impedance of the medium

$\sqrt{\mu r / \mathcal{E} r}$ is dependent of the material properties. Nonetheless, commercially available and natural magnets at frequencies above 500MHz becomes perfect absorbers and therefore are very lossy while at lower frequencies they act as impedance surfaces. This is because at lower frequencies (<500MHz), magnetic materials exhibit domain wall resonance (Dionne, 2003) as shown in figure 9, than gyromagnetic resonance. At gyromagnetic resonance, the permeability goes down to very low values, which shows that not only the boundary displacements but also rotation of domains is affected at these frequencies. Therefore, careful fabrication and alignment of the magnetic moment is required to push domain wall resonances at higher frequency (Volakis, 2009).

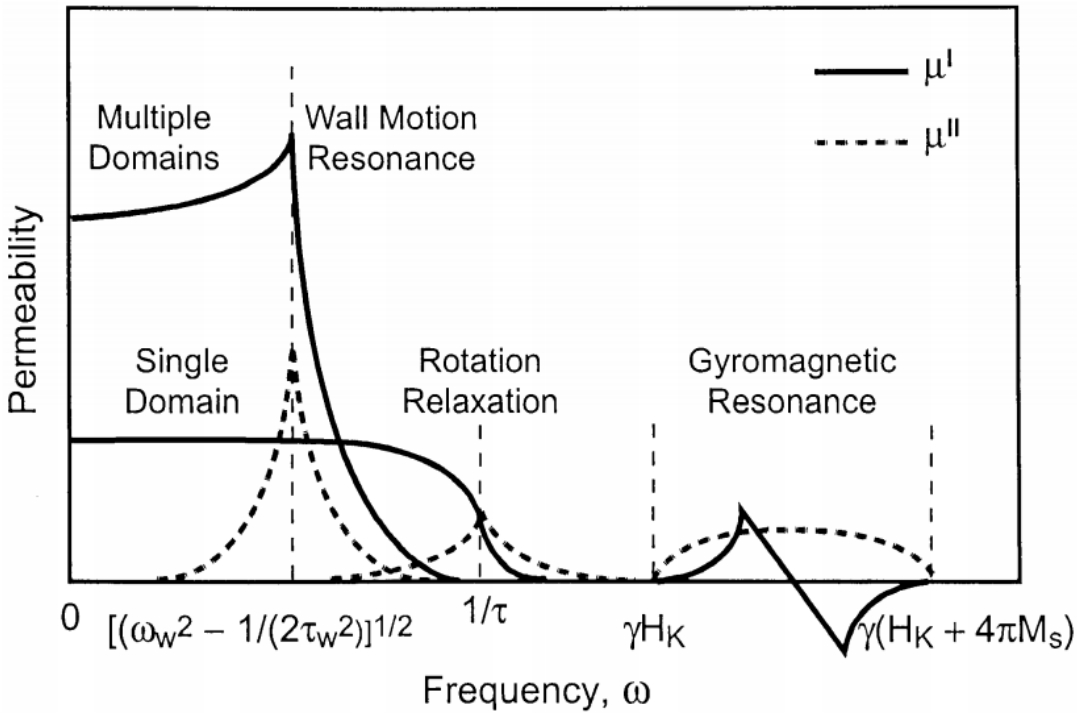

Figure 9: Schematic diagram of permeability variations as a function of frequency caused by various magnetic damping actions. (After (Dionne, 2003)).

Miniaturization through Magnetic material loading

Magnetic material loading of dielectric substrate introduces inductive effect which minimizes loss due to capacitive reactance of the substrate. Recently, artificial high-permeability materials working in the microwave regime (Marqués, 2002), (Gorkunov M. Lapine M., 2002), have been proposed to decrease the size and/or to enhance the impedance bandwidth properties of microstrip antennas (Burke, 2000), (Ziolkowski, 2003) because of the magnetic (inductive) effect introduced by the material. Magnetodielectric materials with $\mathcal{E}_r$ and μ_r greater than one offers much advantage in antenna miniaturization and is the current research focus in the field of antenna miniaturization. Antenna structure incorporating magnetodielectric have been extensively studied in literature. In (Hossein M, 2004) an artificial anisotropic meta-substrate having $\mathcal{E}_r < \mu_r$, made up of layered magneto-dielectric and dielectric materials is designed to maximize the bandwidth of a miniaturized patch antenna, and It is shown that the design of EBG structures utilizing magneto-dielectrics has the dual benefit of improving band-gap rejection levels, while achieving size reduction. (Ikonen P. M., 2006) showed that using a layered substrate containing thin ferromagnetic films, that the radiation quality factor is strongly minimized even in the presence of realistic losses. To minimize loss effect due to magnetic ferrite at high frequency, (Erkmen F. C., 2008), coated the metallic ground plane of antenna with layers of magnetodielectric material, thereby increasing the effective distance between the printed antenna and the magnetic layer. More importantly, the ferrite coating modified the ground plane reflection coefficient between 0 and +1 to enhance conformal antenna radiation even at frequencies when the

distance between antenna and ground plane becomes less than λ/20 (Volakis, 2009). Furthermore, since the characteristic impedance of magneto-dielectric medium is close to that of the free-space $\acute{\eta} = \acute{\eta}_o\sqrt{\mu_r / \mathcal{E}_r}$ it allows for ease of impedance matching over a much wider bandwidth (Hossein M, 2004).

Miniaturization through Dielectric material loading

Antenna miniaturization using high dielectric material loading have been extensively explored. Miniaturization of a printed spiral on the two-different substrate with dielectric values ($^{\varepsilon}_r = 9\ and\ 16$) was studied by (Carver, Microstrip antenna technology, 1981). The miniaturization factor which is a function of thickness, shows a diminishing return after the substrate thickness exceeds 0.1 λ with no observable miniaturization effect after 0.2λ (Volakis, 2009). One major problem associated with high dielectric substrates is that, it enables excitation of surface waves and this leads to low radiation efficiency and high impedance mismatch of the antenna. It also confines most of the excited field in the high permittivity region, leaving only a fraction to be radiated and this reduces the bandwidth of the antenna. To overcome undesirable features of thick and high dielectric substrate in planar antennas without compromising key performance features such as improved bandwidth and radiation efficiency, (Colburn, 1999) adopted the concept of substrate perforation to lower the effective dielectric constant of the substrate figure 1.10. High dielectric material substrate has also been identified to cause impedance mismatch, therefore, care should take when selecting a dielectric material for a particular application.

Motivation

It is desirable for magnetodielectric material to be used in antenna miniaturization be stable and have high permeability over the entire frequency of interest. In most of the RF antenna application reported in literature, ferrites, hexaferrites and their composites with polymer were used as magnetodielectric material to achieve miniaturization. (Shin, 2010.) used ferrite in the design of a monopole antenna for 700MHz LTE band. The antenna showed a low radiation efficiency of 27.9% which was because of a very high significant magnetic loss of 0.189. According to (Han, 2015), Y-type hexagonal ferrites with glass or polymer have been used to realize MD material in (Cheon Y., 2012) and (Lee J. M., 2012).

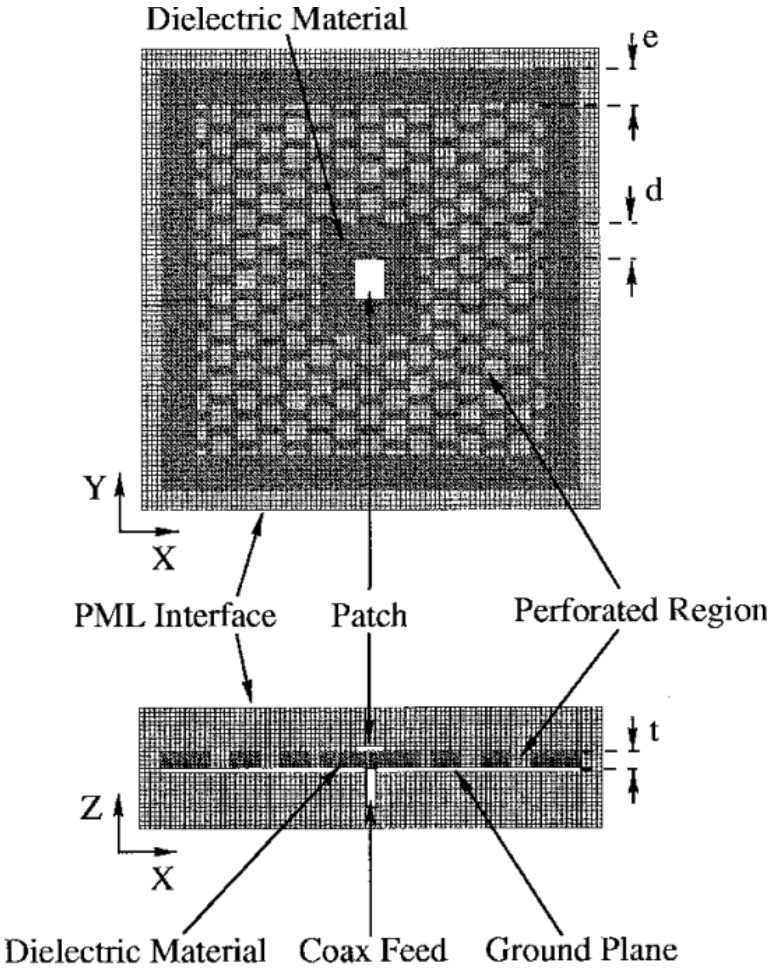

Figure 10: Schematic of the patch antenna on externally perforated substrate on a finite ground plane. The grid represents the FDTD computational cells (after (Colburn, 1999)).

These MD composites showed permeability of ~2 with low magnetic loss at 0.8 ~ 1GHz. With this low loss, antennae in (Cheon Y., 2012)and (Lee J. M., 2012) showed improved radiation efficiencies of 43 and 65% respectively. (Youngs, 2005) blended a ferrite powder and epoxy to form a magnetodielectric composite. The composite showed permeability of 1.56 at 800MHz with 0.035 loss. Radiation efficiency of about 47-82% was measured over the 748-960MHz band. The high radiation efficiency was attributed to

the low loss. However, the thickness of the magnetodielectric composite was 3mm and this resulted in a very low miniaturization factor. Furthermore, for mobile devices, such a thickness is not desirable. The material properties of the magnetodielectric and their antenna performance discussed above are summarized in table 2.

Table 2: Summary of the literature review for the MD material properties and antenna performance (after (Han, 2015))

Material	Permittivity ($\varepsilon_r/\tan\delta_e$)	Permeability ($\mu_r/\tan\delta_m$)	Frequency	Gain (dBi)	Radiation Efficiency (%)	Year
Ferrite compound	3.29/ 0.027	2.01/ 0.189	780MHz	-5.1	27.9	2010 [20]
Y-type hexagonal ferrite + glass	12.7/ 0.0065	2.1/ 0.0474	800MHz	-0.03	43	2012 [21]
Y-type hexagonal ferrite + polymer	5.07/ 0.004	2.01/ 0.03	1GHz	N/A	65 (Simulation)	2014 [22]
Ferrite + epoxy	4.18/ 0.022	1.56/ 0.035	748 – 960 MHz	2.12	82	2014 [23]

Therefore, antenna fabrication on a thinner magnetodielectric material with high permeability and stability at microwave frequency with improved antenna performance is required.

2. ELECTROMAGNETISM AND MAGNETISM IN FERRITE MATERIAL

Introduction

Maxwell's equations are the fundamental equation that guides the theories of electromagnetism. These equations describe how electric and magnetic fields propagate, interact, and how they are affected by objects. Understanding of these equations is critical in antenna design and electromagnetic wave propagation. The equations reveal that isolated charges (positive and negative) produces electric field. If the electric filed is time varying, a propagating electric field is obtained which also produces a propagating magnetic field. Electric charge and the electric current which results from charge motion are ultimately the source of all electromagnetic fields and are included as the source terms in the Maxwell Equations.

$$\nabla \cdot \mathbf{D}(\vec{r},t) = \rho(\vec{r},t) \tag{2.1}$$

$$\nabla \times \mathbf{E}(\vec{r},t) = -\frac{\delta}{\delta t}\mathbf{B}(\vec{r},t) \tag{2.2}$$

$$\nabla \cdot \mathbf{B}(\vec{r},t) = 0 \tag{2.3}$$

$$\nabla \times \mathbf{H}(\vec{r},t) = \mathbf{J}(\vec{r},t) + \frac{\delta}{\delta t}\mathbf{D}(\vec{r},t) \tag{2.4}$$

Equations (2.1) – (2.2) gives the differential form of the Maxwell's equation in 3-dimesional space. These equations are integrated over the entire space or volume to obtain the integral form, equations 2.5 -2.8

$$\oint_s \mathbf{D} \cdot d\mathbf{S} = Q \tag{2.5}$$

$$\oint_c \mathbf{E} \cdot d\mathbf{L} = -\int_s \frac{\delta \mathbf{B}}{\delta t} \cdot d\mathbf{S} \tag{2.6}$$

$$\oint_s \mathbf{B} \cdot d\mathbf{S} = 0 \tag{2.7}$$

$$\oint_c \mathbf{H} \cdot d\mathbf{L} = \int_s (\mathbf{J} + \frac{\delta \mathbf{D}}{\delta \mathbf{t}}) \cdot \mathbf{dS} \tag{2.8}$$

Equations 2.5-2.8 are very important to electrical engineer, the interaction between electromagnetic field and their environment is deduced from these equations. Equation (2.5) implies that the electric flux leaving a volume is proportional to the charge inside the volume. While equation (2.6) suggest that the rate of change of magnetic flux in a closed loop is proportional to the induced voltage in the loop. Equation (2.7) shows that no net magnetic charge exists in a closed surface and equation (2.8) reveals that the integral of magnetic field around a closed loop is proportional to the electric current plus the displacement current.

In other to explain the medium that supports the fields, the constitutive equations that model the properties of the medium are required. These equations show how the flux and intensity terms in Maxwell's equation interact with their environment.

$$\mathbf{D} = \bar{\bar{\epsilon}}\mathbf{E} \tag{2.9}$$

$$\mathbf{B} = \bar{\bar{\mu}}\mathbf{H} \tag{2.10}$$

$$\mathbf{J}_c = \bar{\bar{\sigma}}\mathbf{E} \tag{2.11}$$

For example, if we consider an isotropic environment, the following relations hold

$$\bar{\bar{\epsilon}} = \epsilon \tag{2.12}$$

$$\bar{\bar{\mu}} = \mu \tag{2.13}$$

$$\bar{\bar{\sigma}} = \sigma \tag{2.14}$$

Electrical engineering as an art, is dedicated to finding the physical material (or medium) with desirable properties (μ $and\mathcal{E}$) to force the required electromagnetic response. Our focus in this thesis is finding materials with good magnetic properties that is suitable for microwave applications especially in antenna design.

Magnetism in materials

Materials are often classified according to how then respond to an externally applied magnetic field. Observation of how the magnetic moments are arranged in a material, helps to identify different kinds of magnetisms that exist in nature. Figure 11 shows the five broad categories of magnetic behavior exhibited by materials.

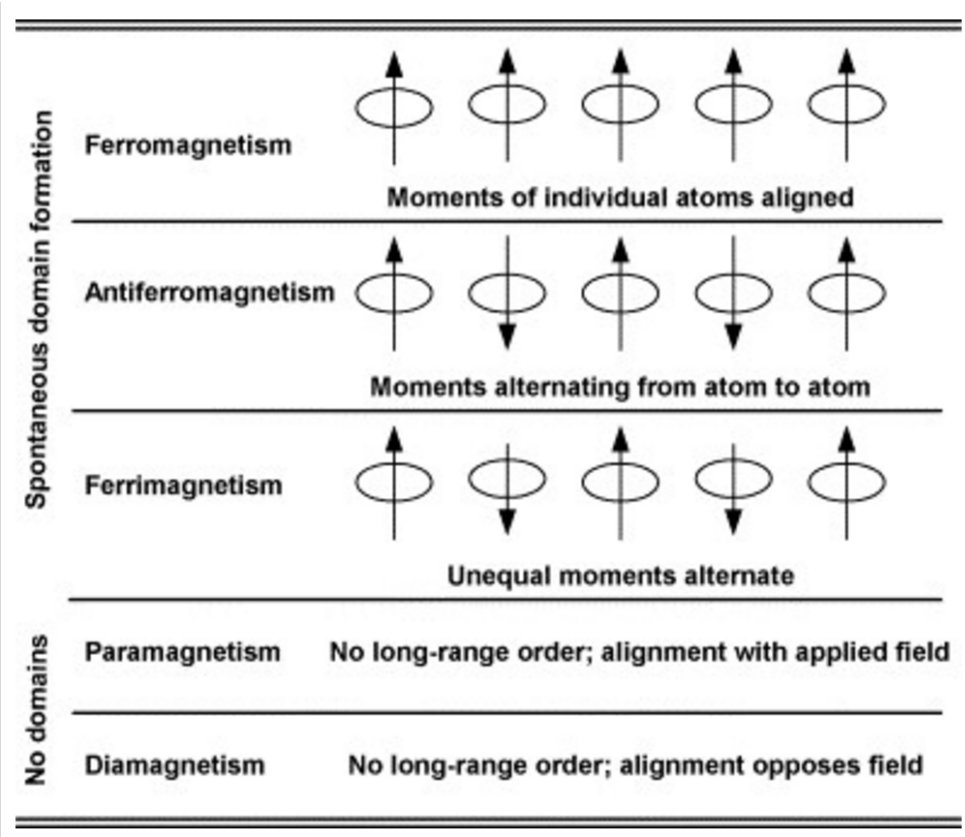

Figure 11: Different magnetic behavior in materials

Ferromagnetism

This is the strongest form of magnetism. It is a mechanism by which materials form permanent magnets. A ferromagnet has a spontaneous magnetic moment, i.e. a magnetic moment even in zero applied magnetic field. Ferromagnetic materials such as Iron, nickel, cobalt and some of the rare earths have aligned atomic magnetic moments of equal magnitude and their crystalline structure allows for direct coupling interactions between the moments, which may strongly enhance the flux density (gadolinium, dysprosium). They also exhibit long ordering at atomic level and this causes the unpaired electrons to align (in one direction) together into regions know as magnetic domain. In bulk materials, these domains are randomly oriented with respect to each other and that causes the material to be unmagnetized. However, in the presence of an external magnetic field, these domains realign itself and the material becomes magnetized. Ferromagnetic materials exhibit hysteresis and usually have high permeability. They also exhibit remanence which is an important factor in permanent magnets. The ferromagnetic behavior of materials is dependent on temperature. The Curie temperature is the boundary between the ferromagnetic behavior and paramagnetic behavior in materials. Above this temperature, the material loses its long order arrangement and hence it is important factor to consider in material selection. The temperature dependence of magnetization in some ferromagnetic materials is summarized in table 3. Ferromagnetic materials are indispensable in industry and modern technology, and are the basis for many electrical and electromechanical devices such as: electromagnets, electric motors, generators, transformers, and magnetic storage (e.g., tape recorders and hard disks).

Table 3: Magnetization of Ferromagnetic crystals

Substance	Magnetization M_s, in gauss		n_B(0 K), per formula unit	Curie temperature, in K
	Room temperature	0 K		
Fe	1707	1740	2.22	1043
Co	1400	1446	1.72	1388
Ni	485	510	0.606	627
Gd	—	2060	7.63	292
Dy	—	2920	10.2	88
MnAs	670	870	3.4	318
MnBi	620	680	3.52	630
MnSb	710	—	3.5	587
CrO_2	515	—	2.03	386
$MnOFe_2O_3$	410	—	5.0	573
$FeOFe_2O_3$	480	—	4.1	858
$NiOFe_2O_3$	270	—	2.4	(858)
$CuOFe_2O_3$	135	—	1.3	728
$MgOFe_2O_3$	110	—	1.1	713
EuO	—	1920	6.8	69
$Y_3Fe_5O_{12}$	130	200	5.0	560

Antiferromagnetism

Antiferromagnetic materials (AFM) also exhibit long ordering in atomic level and this causes the magnetic moment to align in an antiparallel (opposite direction) manner. The exchange interaction couples the moments such that they are antiparallel therefore leaving a zero-net magnetization below the Néel temperature (Sorensen K.J., 2001). Above the Neel temperature (T_N) thermal energy is sufficient to cause the equal and oppositely aligned atomic moments to randomly fluctuate leading to a disappearance of their long-range order. In this state, the material exhibits paramagnetic behavior. Antiferromagnetism is common among transition metal compounds, especially oxides. Examples include hematite, metals such as chromium, alloys such as iron manganese (FeMn), and oxides such as nickel oxide (NiO). These materials are used in magneto-

resistive RAM. Above T_N, the susceptibility of AFM obeys the Curie-Weiss law for paramagnets but with a negative intercept indicating negative exchange interactions figure 12.

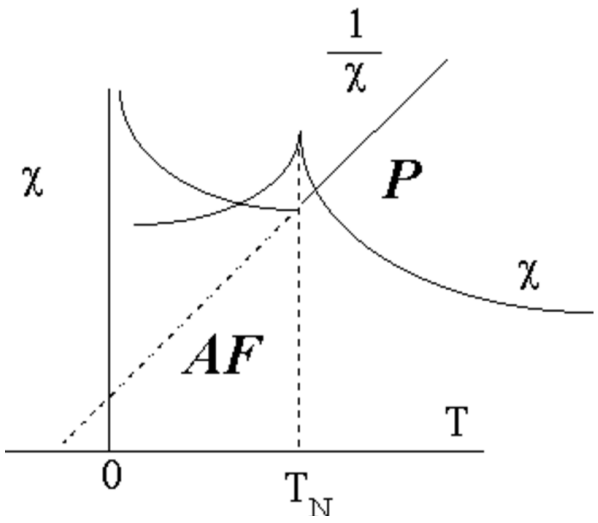

Figure 12: Antiferromagnetic Susceptibility against temperature

Table 4: Antiferromagnetic crystals and their temperature profile

Substance	Paramagnetic ion lattice	Transition temperature, T_N, in K	Curie-Weiss θ, in K	$\frac{\theta}{T_N}$	$\frac{\chi(0)}{\chi(T_N)}$
MnO	fcc	116	610	5.3	$\frac{2}{3}$
MnS	fcc	160	528	3.3	0.82
MnTe	hex. layer	307	690	2.25	
MnF_2	bc tetr.	67	82	1.24	0.76
FeF_2	bc tetr.	79	117	1.48	0.72
$FeCl_2$	hex. layer	24	48	2.0	<0.2
FeO	fcc	198	570	2.9	0.8
$CoCl_2$	hex. layer	25	38.1	1.53	
CoO	fcc	291	330	1.14	
$NiCl_2$	hex. layer	50	68.2	1.37	
NiO	fcc	525	~2000	~4	
Cr	bcc	308			

Ferrimagnetism

Ferrimagentic material just like the antiferromagnetic exhibit long ordering in atomic level and this causes the magnetic moment to align in an antiparallel (opposite direction) manner. Unlike ferromagnetic materials, in ferrimagnetic materials, the opposing moments are unequal and a spontaneous magnetization remains. This happens when the populations consist of different materials or ions (such as Fe^{2+} and Fe^{3+}). These are materials are of great interest to engineers. Like the ferromagnetic materials, they hold spontaneous magnetization below the curie temperature and show paramagnetic behavior above it. However, below the curie temperature, there is a temperature known as the magnetization compensation point at which the opposing magnetic moment becomes equal and hence cancel out resulting in zero net magnetization. This compensation point is a crucial point for achieving high speed magnetization reversal in magnetic memory devices (Stanciu, 2006).

Ferrimagnetism is exhibited by ferrites and magnetic garnets. The oldest known magnetic substance, magnetite (iron (II, III) oxide; Fe_3O_4), is a ferrimagnet; it was originally classified as a ferromagnet before Néel's discovery of ferrimagnetism and antiferromagnetism in 1948 (Néel L., 1948). Known ferrimagnetic materials include YIG (yttrium iron garnet), cubic ferrites composed of iron oxides and other elements such as aluminum, cobalt, nickel, manganese and zinc, hexagonal ferrites such as $PbFe_{12}O_{19}$ and $BaFe_{12}O_{19}$, and pyrrhotite, $Fe_{1-x}S$. This class of materials are commonly used for microwave frequency applications. They have high resistivity which means they prevent eddy current flow and shows magnetic anisotropy when induced by an eternal

field and therefore are used to manufacture microwave devices like circulators, isolators etc. They are also used to produce optical isolators and circulators.

Paramagnetism

This class of materials have no long-range order. Although, some of the atoms or ions of these materials have net magnetic moment due to unpaired electrons in partially filled orbitals. These individual magnetic moments do not interact together magnetically and hence resulting in zero net magnetization. However, in the presence of an external field, these atomic magnetic moments begin to interact and align in the direction of the filed resulting in a net positive magnetization and susceptibility.

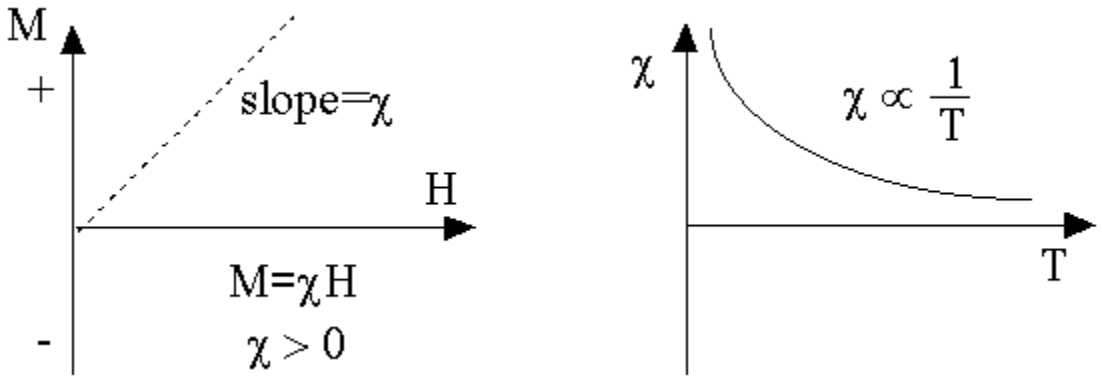

(a) (b)

Figure 13: Paramagnetism (a) magnetization vs applied filed. (b) Susceptibility vs temperature

Diamagnetism

Diamagnetism is an inherent property of every material. although it is usually very weak because of non-interaction between orbiting electrons in the presence of an external field. The orbital shells of the atoms are filled up and hence they have no net magnetic moment. Furthermore, in the presence of an external field, the magnetic

moments align in opposite direction to counter the effect of the field resulting in negative magnetization susceptibility figure 14.

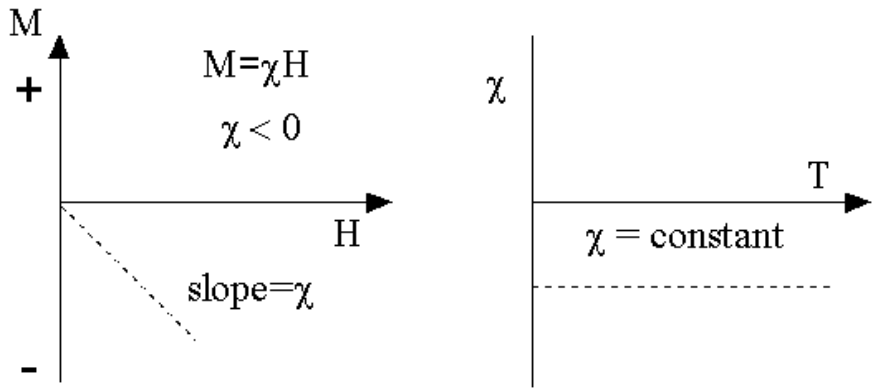

Figure 14: Diamagnetism (a) magnetization vs applied filed. (b) Susceptibility vs temperature

To further understand the magnetic behavior of material, we take a closer look at the sub-atomic levels of this materials. Below the Neel and Curie temperatures, antiferromagnetic and ferromagnetic materials respectively, spontaneously divide into smaller regions known as domains figure 15. The magnetization in each domain points in the same direction which may be different from other domains.

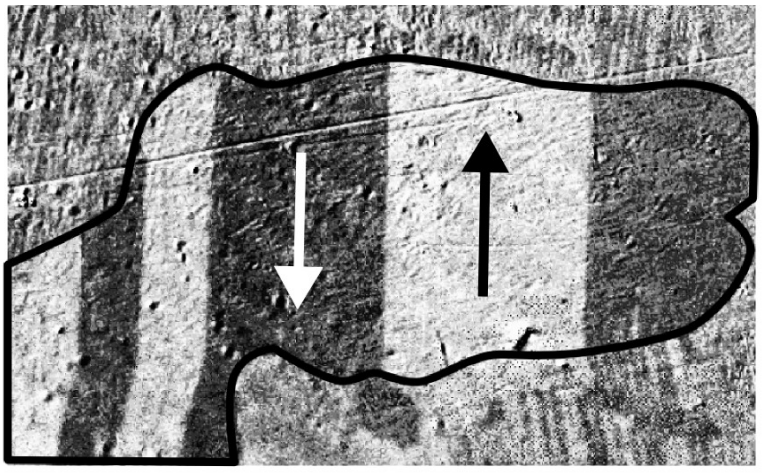

Figure 15: Orientation of the domains separated by domain walls.

The magnetic domain is responsible for magnetic properties in most materials, such as attraction to a magnetic field, forming a permanent magnet etc. The commonly measured magnetic material properties illustrated in the hysteresis loop (figure 16) could the explain using the domain wall theory.

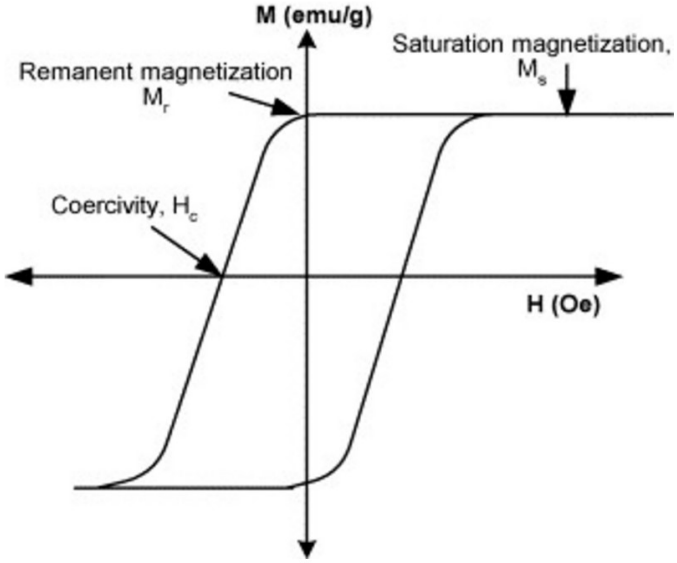

Figure 16: Hysteresis loop of a multidomain magnetic material.

Where H is the filed amplitude in Oe and M is the saturation in emu/g

When an external field is applied to a magnetic material, the field increases the exchange bias in the material which causes the atomic spin to align in the direction of the filed. As the field increases, the material attains a maximum magnetization known as saturation magnetization M_s. However, as the magnitude of the field decreases, the spin does not always align with decreasing field and therefore has a residual magnetism at zero field know as remanent magnetization M_r. As the amplitude of the field continues to increase in the negative direction, coercive force H_c is applied bring the material back to zero magnetization.

Magnetism and Structure of Ferrite Materials

Ferrites are ceramic materials of iron(III) oxide (Fe_2O_3) combined chemically with one or more additional metallic elements. They exhibit ferrimagnetism and are electrically nonconductive. They can be divided into two categories based on their resistance to being demagnetized. Soft ferrites have low coercivity and are by far the most widely used ferrite for microwave applications and in manufacturing of soft core for inductors and transformers. Hard ferrites on the contrary requires high coercive force to be demagnetized. According to their crystal structure, ferrites are divided into two groups know as spinels and garnets. Complete classification of ferrites is not within the scope of this work but could be find in ((Mahmoud Goodarz Naseri, 2012)).

Spinel ferrites have found great use in microwave applications and therefore are the focus of this thesis. Magnetic materials with low loss at microwave frequency is not common. Natural magnets tend to have high loss at microwave frequency because of the gyromagnetic resonances exhibited by the mechanical atomic system. At excitation frequencies, far below magnetic resonance the magnetic materials align their internal magnetic fields to track the applied field. At low frequency, the relative permeability tends to stay constant but as the frequency increases to resonant frequency, the atomic magnetic resonance does not track the field effectively and at frequencies above resonant, the atomic system completely loses track of the excitation field and causes the magnetic moment arrangement to be random, hence, makes the material effectively non-magnetic high above resonance and μr approaches 1.

As noted before, spinels have unique properties which could be attributed to their unique crystal structure. Their structure is typically of the form $MeFe_2O_4$, where *Me* refers to the metal, and can be described as a cubic close-packed arrangement of oxygen atoms, with Me^{2+} and Fe^{3+} at two different crystallographic sites. These sites have tetrahedral and octahedral oxygen coordination (termed as A and B-sites, respectively), so the resulting local symmetries of both sites are different (Daliya S. Mathew, 2007). Figure 17. shows the structure a spinel.

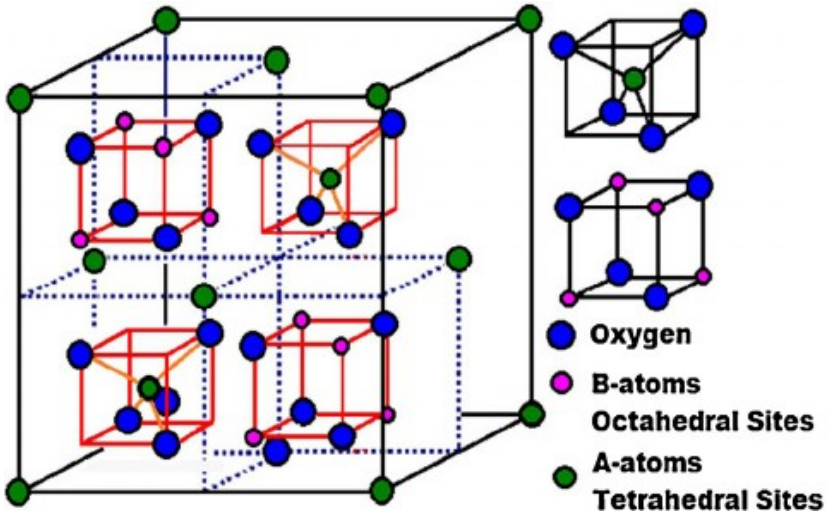

Figure 17: Schematic of unit cell for a spinel structure

The A and B sites are occupied by metal cation. The metal cation in the A site is tetrahedrally bonded with oxygen while the metal cation in B site bonds with oxygen octahedrally. When the A and B sites are occupied by the Me^{2+} cations and Fe^{3+} cations respectively, the ferrite is called a normal spinel. However, some ferrite materials exhibit inverse ordering in which the A site is occupied by the Fe^{3+} and the site by Me^{2+}, this arrangement is known as the inverse spinel. While in many others, cation distribution possesses an intermediate degree of inversion where both sites contain a fraction of the

Me^{2+} and Fe^{3+} cations. Magnetically, spinel ferrites display ferrimagnetic ordering. The magnetic moments of cations in the A and B-sites are aligned parallel with respect to one another. Between the A and B-sites the arrangement is antiparallel and as there are twice as many B-sites as A-sites, there is a net moment of spins yielding ferrimagnetic ordering for the crystal. The choice of metal cation and the distribution of ions between the A and B-sites therefore, offer a tunable magnetic system (Vestal, 2004).

Magnetic moments in materials are believed to be because of combine effect of the electron spin and the orbital angular momentum state and varies depending on whether atoms in one region are aligned with atoms in another. Orbital motions in atoms constitutes tiny loops of current known as magnetic dipoles. These dipoles interact with the electron spin, giving rise to spin-orbit coupling. The measure of this coupling is known as *Lande g-factor,* and is a very important parameter to consider while choosing ferrite materials. A *Lande g-factor* of unity implies magnetic moment due to orbital motion while a value of two implies moment due to electron spin.

Ferrite material in magnetic field

As stated earlier, in presence of an external magnetic field, magnetic moment in ferrites begin to align in the direction of the applied field. For this to happen, a strong field ($\sim 10^8$A/m) is required to overcome the energy of the thermal agitation which tends to counter the field effect. Ferrites responds to external magnetic field by acquiring magnetization $\vec{M}$. This analogous to the polarization in dielectrics under external electric field. However, unlike the dielectric, magnetization in magnetic material is a non-linear function of magnetic field. The magnetization is related to the magnetic field intensity $\vec{H}$ by

$$\vec{M} = x\,\vec{H} \qquad (2.15)$$

$$\vec{B} = \mu\,\vec{H} \qquad (2.16)$$

$$\mu = x + 1 \qquad (2.17)$$

Where x is the magnetic susceptibility.

μ is magnetic permeability.

For a constant x, equation 2.15 becomes a linear function of $\vec{M}$ and $\vec{H}$. The susceptibility by itself is a function of $\vec{H}$ in ferromagnetic material and hence equation 2.15 is non-linear. The magnetic flux density $\vec{B}$ is also a non-linear function of magnetic field as shown in equation 2.16. These relationships are depicted in figure 18

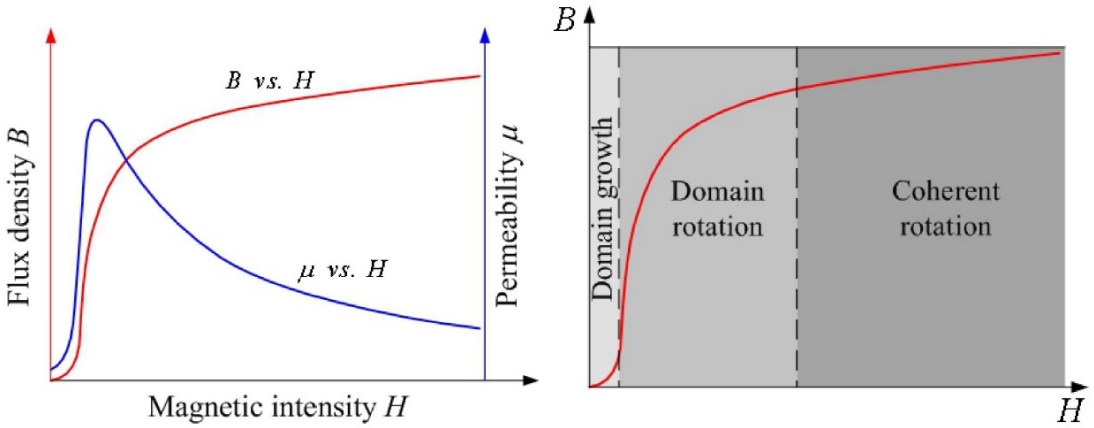

Figure 18: Magnetic flux density dependence of magnetic field intensity.

3. METHOD OF PREPARING A POLAR BASED MAGNETIC INK SUITABLE FOR INKJET PRINTING AND CHARACTERIZATION OF NI-ZN AND MN FERRITE THIN FILM

Introduction

Ferrite materials e.g. spinels and garnets, have attracted a lot of research interest in recent time because of its excellent microwave frequency characteristics such as low magnetic loss. As discussed in previous chapters, scholars are beginning to gain a deeper insight in the chemistry of these materials and understanding of the physics behind their behavior in different media under different conditions.

The importance of ferrite inclusion in antenna structure has been discussed in previous chapters. It is a well-established fact, that natural magnets exhibit high loss at high frequency because of the gyromagnetic resonances exhibited by the mechanical atomic system. The magnetic moment of these materials tends to misalign with the applied field at microwave frequency and therefore, the overall permeability of the system is reduced. In lieu of natural magnets, engineering of artificial materials known as meta-materials, to force the desired response at microwave frequency and in antenna application is the main stream of research focus nowadays.

Since its introduction into main stream electronic device manufacturing, inkjet printing has become a preferred choice in device fabrication technology. This is due to its low fabrication and material conservation cost compare to traditional photolithographic process. Furthermore, it is an additive technique which makes it more suitable for many applications compared to conventional, subtractive photolithographic technique. Inkjet printing is a non-contact reprographic technique which enables light-weight, conformal, and large aperture antennas possible at low cost. When operated on drop-on-demand mode (DOD), it has

high placement accuracy and the inks are dropped only on specified locations on the substrate and therefore it can be used for all kinds of substrates. Its low temperature process makes it suitable and an efficient method in flexible electronic circuit manufacturing.

Nanoparticles have unusual electrical, mechanical, optical properties etc. compared to the bulk material, therefore, desirable magnetic properties of ferrites could be engineered at sub-micron level and are easy to control. Hence, different deposition techniques such as pulse laser deposition (PLD), chemical vapor deposition (CVD), molecular beam epitaxy (MBE) etc. have been used to deposit thin films of ferrite on substrates for different applications. (Wang, 2004) deposited cobalt ferrite ($CoFe_2O_4$) thin films on $CoCr_2O_4$buffered $SrTiO_3$ and $MgAl_2O_4$ substrates using pulse laser deposition (PLD) technique. Cobalt ferrite thin film was found to show more Magnetic anisotropy than the bulk material. However, in this thesis, our focus is on synthesis of polar based ferromagnetic ink suitable for inkjet printing and characterization of Nickle-Zinc and Manganese ferrites thin films.

Method of preparing magnetic ink

The magnetic ink belongs to the class of ferrofluids which contains magnetic particles with a polar surface-active agent known as surfactants, adsorbed on the particle surface and thereafter dispersed in an aqueous medium also referred as carrier. Ferrofluid has found great interest in the field of fluid dynamics, biomedical and other engineering applications. Depending on the proportion of suitable components and hydrophile–lypophile balance (HLB) value of the surfactant used, the formation of microdroplets can be in the form of oil-swollen micelles dispersed in the aqueous phase or water-swollen

micelles dispersed in oil (Daliya S. Mathew, 2007). The HLB value of surfactants is therefore, a very critical parameter in magnetic ink preparation. Figure 19 shows the HLB chart showing surfactant function.

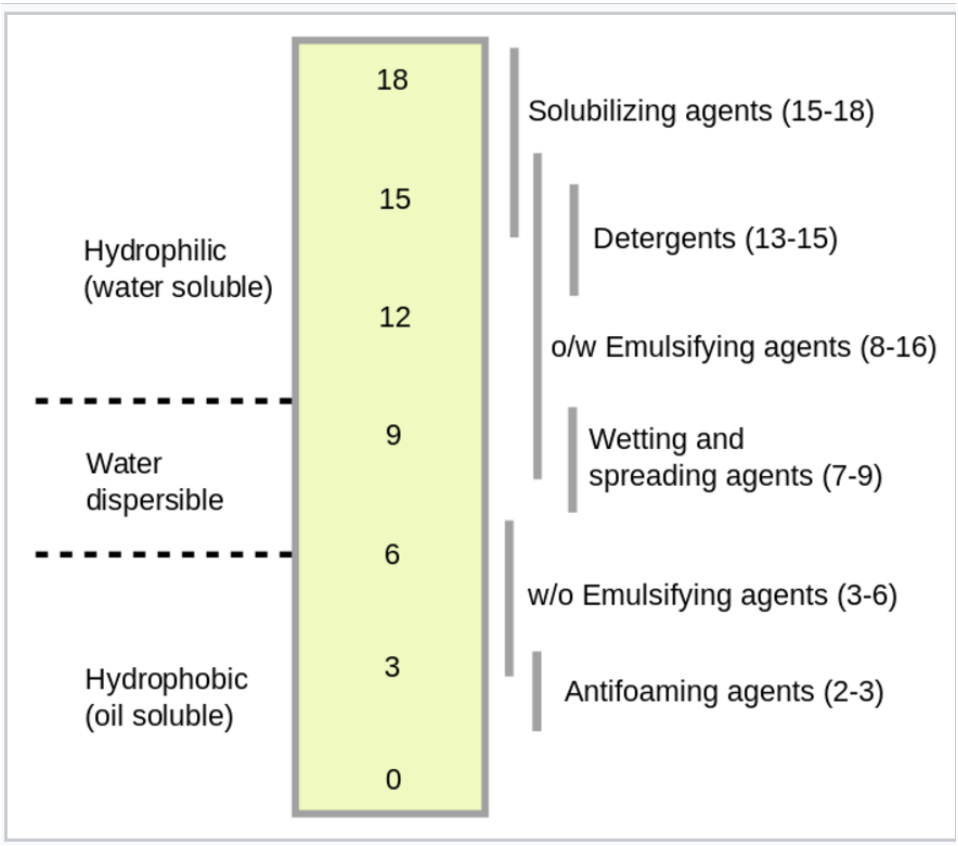

Figure 19: HLB scale showing surfactant functions

As stated earlier, a ferrofluid is typically made by suspending monodomain ferromagnetic particles of size 10nm to 150nm, in a nonmagnetic liquid carrier. The particle size is critical because ferrites with heavy particles are difficult to suspend in liquid carrier. Also, understanding the parking parameter of the emulsifier enables for the control of the micelle aggregate and the formation of uniformly dispersed ink. The parking parameter is given by the ratio *v/al,*

Where v is the emulsifier hydrocarbon volume, *a* the polar head area and *l* is the fully extended chain length of the emulsifier. When the ratio v/al is larger than unity, the aggregate curvature will be towards water. This corresponds to a situation where the oil is penetrating the emulsifier tails and/or the electrostatic repulsion between the charged head group is low. When the ratio is less than unity we have a situation where the electrostatic repulsion is larger and/or the oil is not penetrating the emulsifier tails. Spherical direct micelles are formed when the packing parameter is less than 1/3. The limiting values for packing parameters for cylinders and planer bilayers are 0.5 and 1, respectively (Daliya S. Mathew, 2007). These surfactant-covered water pools offer a unique microenvironment for the formation of nanoparticles. They not only act as microreactors for processing reactions but also exhibit the process aggregation of particles because the surfactants could adsorb on the particle surface when the particle size approaches to that of the water pool. As a result, the particles obtained in such a medium are generally extremely fine and monodisperse (Paul, 1997).

The magnetic material of interest in this thesis belongs to the group known as magnetite (Fe_3O_4), typically to those with γ-Fe_2 O_3 and their likes. They exhibit strong ferromagnetism with properties that are nearly isotropic; they often show low coercivity, low hysteresis loss, high permeability, and high electrical resistivity. The finely divided magnetic materials are more or less permanently suspended in a liquid medium with the help of a dispersing agent, a surfactant and the likes to form a uniform, stable and highly dispersed magnetic fluid. The surfactant prevents particle agglomeration while the Brownian motion prevents particle sedimentation in magnetic or gravitational field. The surfactant usually has molecular structure that includes a water-soluble or hydrophilic

component, and a water insoluble or hydrophobic component. The hydrophobe is usually the equivalent of a hydrocarbon having from about 8 to 18 carbons, and can be aliphatic, aromatic, or a mixture of both. The sources of hydrophobes are normally natural fats and oils, petroleum fractions, relatively short synthetic polymers, or relatively high molecular weight synthetic alcohols, and the like. The hydrophilic groups give the primary classification to surfactants, and are categorized as anionic, cationic or non-ionic in nature. The anionic hydrophiles generally belong to a group including carboxylates (soaps), sulphates, sulphonates, phosphates, and the like. The cationic hydrophiles are generally a form of an amine product. The non-ionic hydrophiles associate with water at the ether oxygens of a polyethylene glycol chain. The hydrophilic end of the surfactant is strongly attracted to the water molecules of an aqueous solution. The force of attraction between the hydrophobic component of the surfactant and the water is only slight. As a result, the surfactant molecules align themselves at the surface and internally so that the hydrophile end is oriented toward the water and the hydrophobe is oriented away from the water. This internal group of surfactant molecules is referred to as a micelle (McElligott, 2004). Essentially, the surfactant acts like a trap for the ferrite nanoparticles and aid in their dispersion. For water based magnetic ink, the surface coated nanoparticles are dispersed in water. However, in non-aqueous based ink, the surface coated nanoparticles could be dispersed in any of the nonmagnetic liquid carrier such as those belonging to the aliphatic hydrocarbons e.g. kerosene, heptane, octane, cyclooctane, decane, mineral oil etc. or halogenated hydrocarbons such as carbon tetrachloride or trichloroethylene and aromatic solvents such as benzene, toluene and their non-polar derivatives.

Nickle-Zinc ferrite and Manganese ferrite ink preparation

To illustrate the method of magnetic ink preparation described above, we prepared samples of magnetic ink containing nickel-zinc ferrite and manganese ferrite as follows: A colloidal solution of the ferrite comprising of $MnFe_2O_4$ (or NiZn) and having an average particle size of 50nm with a melting point greater than 300C was prepared by wet method using Terpinol. An aqueous solution of sodium Oleate prepared by adding 0.4g of the salt in 30ml of water followed by ultasonication of the salt solution for 30mins at 40C to enable complete dissolution of the salt, was thereafter added to the colloidal solution of the ferromagnet. The mixture was subjected to a steady but mild vibration in an ultrasonication bath for 3hours at 40C. This allows for the complete coating of each ferromagnetic particle with a monolayer of the oleate salt by adsorption. The PH of the mixture is preferred to maintain a value between 8-10.

Thereafter, HCL was added to the mixture to adjust the PH to a value slightly acidic between 5-6. This is an important step because it aids the precipitation of the coated particle from the solution by flocculation. Any other acid could be used to achieve the same result, the acid only changes excess of the unsaturated fatty acid ion in the oleate salt to free molecules which plays no role in the formation of a colloidal dispersion. Thereafter, the coated ferrite particle is separated from the solution by filtration or decantation, centrifugation but most preferably centrifugation and thereafter washed with water to remove excess of the acid.

Thereafter the coated ferrite particle was peptized in water using sodium deodocylsulphate (SDS) or any nonionic surfactant having a Hydrophile-Lipophile Balance (HLB) >10 e.g. TRITON X-45, TRITON X-100, those containing phosphate,

sulphate or sulfonate radical etc. or those belonging to any of ether, ester or alkylphenol with 8-17 carbon atoms. The HLB value is critical for sufficient dispersion of the ferrite particles in water.

The viscosity of the ink can be varied between 1-10cP by addition of appropriate amount of water. For inkjet printing, a viscosity of about 5cP is preferred and dispersed magnetic particle in the ink should be kept in range between 3% to 20% by weight of the composition.

Characterization of Ni and Mn Ferrite ink

The synthesized Ni-Zn ferrite and Mn-ferrite ink samples used in this thesis was characterize after preparation. The inks have a Ph value and total dissolved solute (TDS) of about 6.3, 3.78 mS and 5.9, 4.2 mS respectively, the Ph values were measured using OAKTON Ph meter and a viscosity of about 7 cPa, 7.4 cPa respectively, measured using Rheosense m-Vroc. The surface tension of the ferrite inks is about 30mN/m as shown in figure 20 which shows that it can easily form a shape.

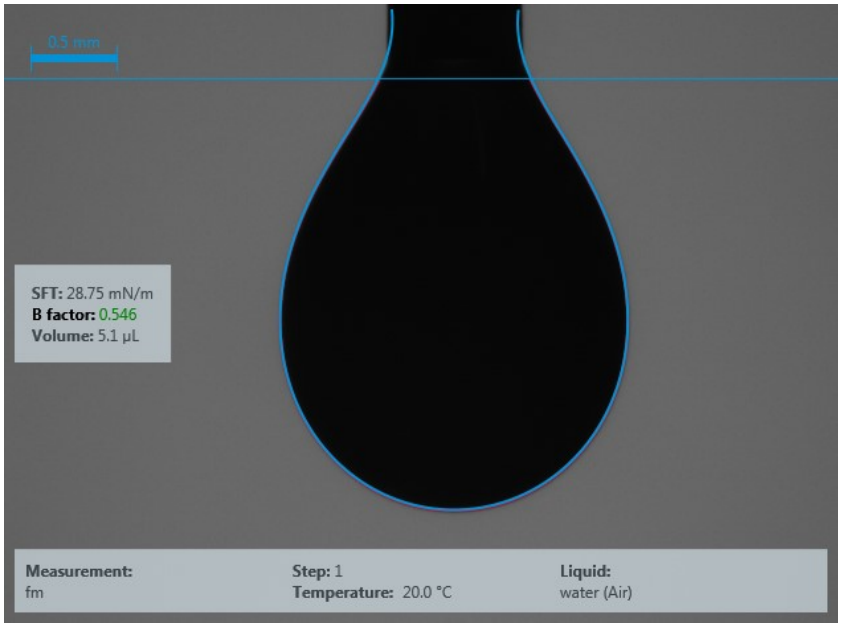

Figure 20: Surface tension of ferrite inks

These values of viscosity and surface tension makes it suitable for inkjet printing. The ink has excellent jettability and uniform droplets when used in Dimatix 2800 Inkjet printer, having approximately 21.5 µm nozzle size and nozzle - nozzle spacing of 254 microns. It also shows a very good adhesion on different substrates such as flexible kepton polyimide, silicon and gallium-arsenide wafers.

Furthermore, the magnetic properties of the inks were measured using a vibrating sample magnetometer (VSM). The saturation magnetization of Mn-ferrite ink at 300K was 62 emu/cm^3 figure 21. According to figure 21, Manganese ferrite ink exhibits a very low coercivity and therefore has low hysteresis loss at high frequency which is desirable for microwave frequency applications. It also shows very high resistivity and can be used in applications where eddy current loss is a big concern. However, the ink is not suitable in making memory devices because of the extremely low remanence.

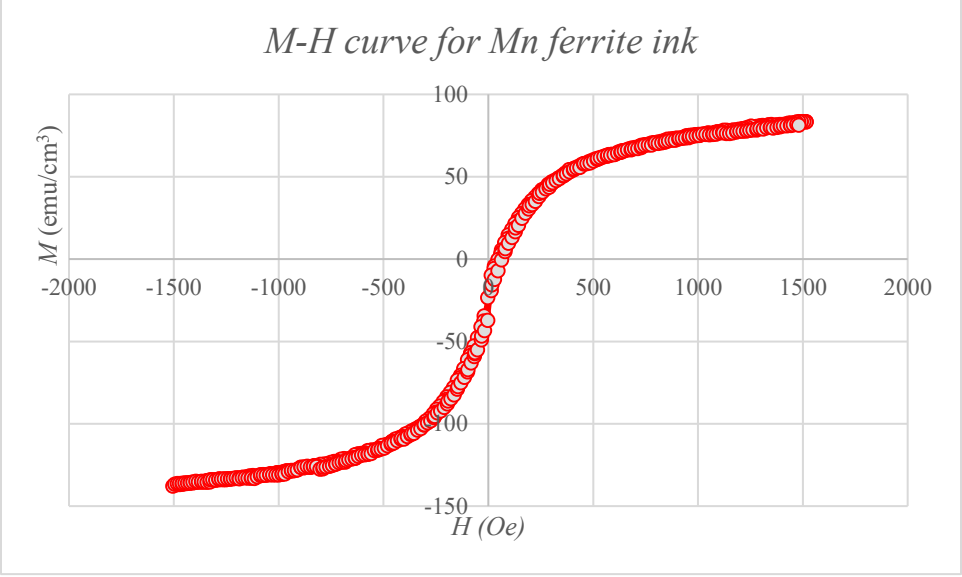

Figure 21: M – H curve for Mn ferrite ink

As could be seen, it also shows a moderate magnetization in low magnetic field but the magnetization is believed to increase significantly at high fields. The reason for this low

magnetization at low fields could be attributed to the shell-core morphology of the coated ferrite particles.

Various samples of both Mn-ferrite and NiZn ferrite thin films with thickness raging form 5um to 25um were printed on three different substrates. Figures 22 and 23 shows a power microscopic image of Mn-ferrite thin film printed on 100mm diameter, 625um thickness, semi-insulating and n-type gallium arsenide wafer (GaAs) and thickness measurement using profilometer. Although different samples were prepared both on kepton polyimide, silicon wafer substrates, uniform films were obtained on all substrates but this thesis is focused on reporting results on GaAs because of its application in fabrication of high frequency devices (wireless communication), Hetero-junction Bi-polar Transistor (HBT), pseudomorphic High Electron Mobility Transistor (pHEMT) etc.

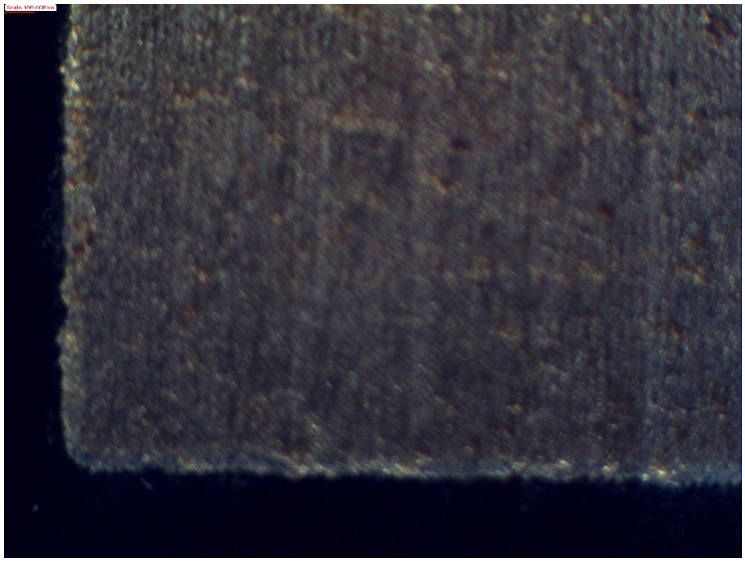

Figure 22: Microscopic image of Mn-ferrite thin film printed on GaAs.

The profilometer measurements of the thin film is shown below:

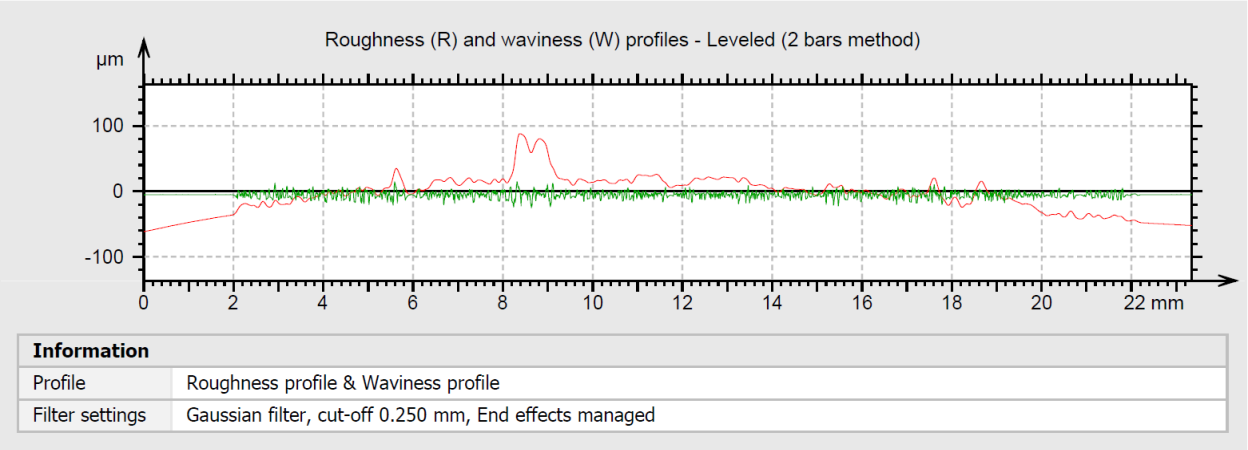

Figure 23: Roughness and Waviness profile of Mn-ferrite on GaAs

The roughness and waviness profile of the thin film was measured using a gaussian filter with 0.250mm cut-off, figure 23. An arithmetic mean roughness *Ra* of 0.0278 was obtainned along other roughness values (Rp and Rq) as shown in figure 25. It is shown that the thin film surface is relatively smooth which means no irregularities on the surface and no formation of nucleation sites for cracks or corrosion. It also shows that the surface is compact and will form a robust unit when intergrated with other circuit componenets.

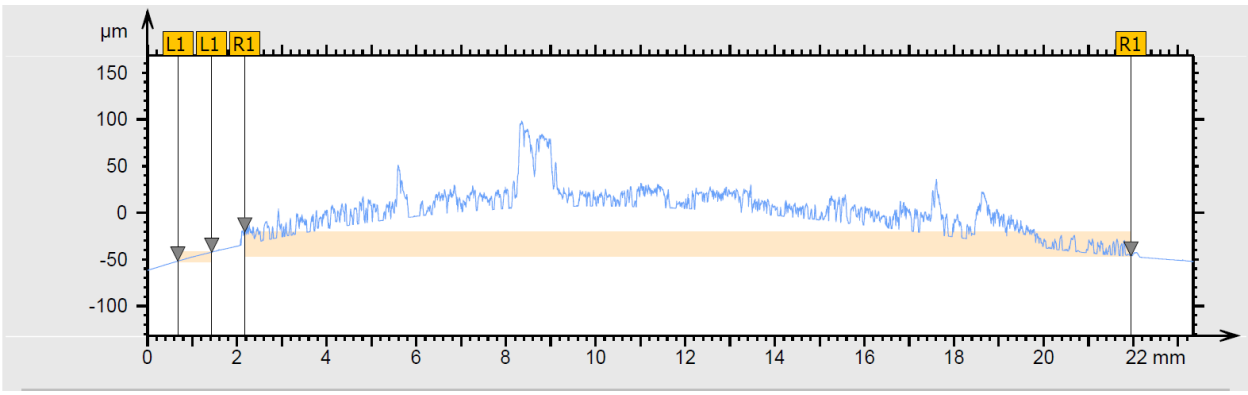

Figure 24: Thickness measurement of Mn-ferrite on GaAs

ISO 4287			
Amplitude parameters - Roughness profile			
Ra	0.0278	µm	*Gaussian filter, 0.25 mm*
KLA-Tencor Parameters			
P15 Roughness profile parameters			
MaxRa	0.0697	µm	*Gaussian filter, 0.25 mm*
ISO 4287			
Amplitude parameters - Roughness profile			
Rq	0.0543	µm	*Gaussian filter, 0.25 mm*
Rp	0.749	µm	*Gaussian filter, 0.25 mm*
Amplitude parameters - Waviness profile			
Wa	4.80	µm	*Gaussian filter, 0.25 mm*
Wq	5.55	µm	*Gaussian filter, 0.25 mm*
Wp	8.99	µm	*Gaussian filter, 0.25 mm*

Figure 25: Summary of roughness and waviness measurement of Mn-Ferrite on GaAs

Because of the importance of surface profile of the thin film on antenna performance, we further investigated the surface morphology of the ferrite film using atomic force microscopy.

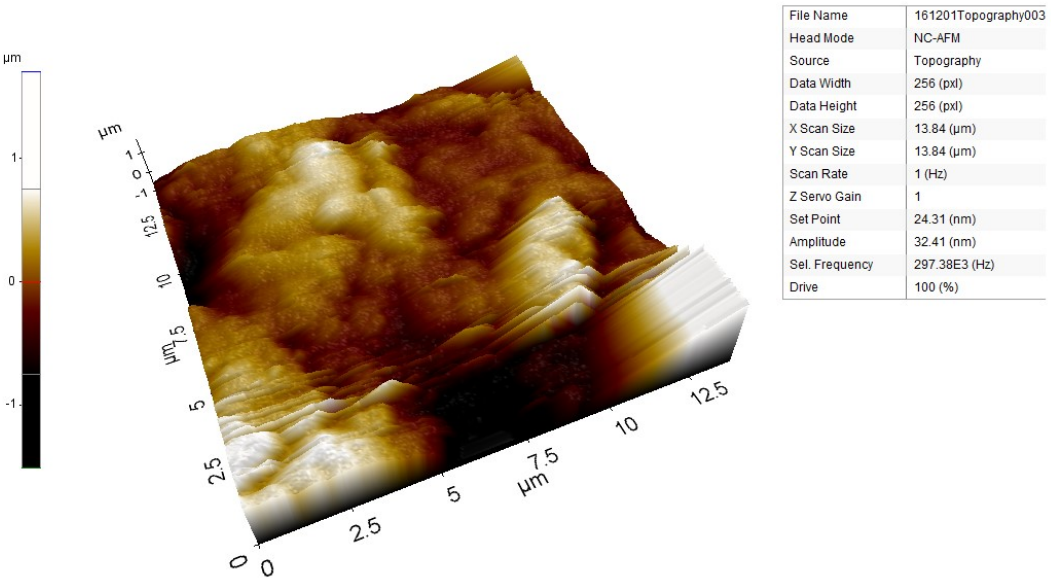

Figure 26: AFM image of Mn-ferrite film

The AFM scan was performed in non-contact mode operation over 13.84um X 13.84um scan size. The image further revealed the smoothness of the ferrite morphology.

The material properties ($\mathcal{E}r$ *and* μr) of the ferrite films were extracted using microstrip transmission line permeameter.

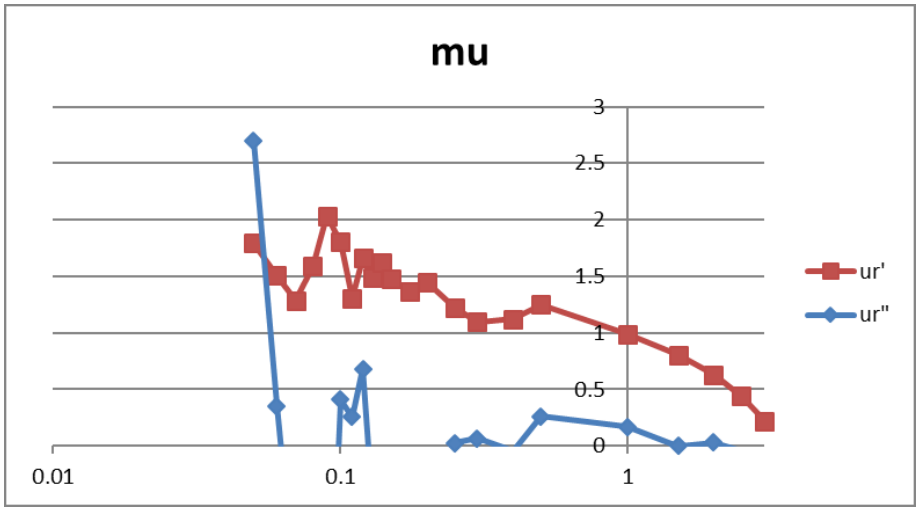

Figure 27: Permeability measurement of Mn-ferrite thin film

The thin film sample within the frequency range of 10MHz-1GHz, attained a relative permeability of 2 at about 100MHz as shown in figure 27. The permittivity at this frequency was stable at 50, figure 28.

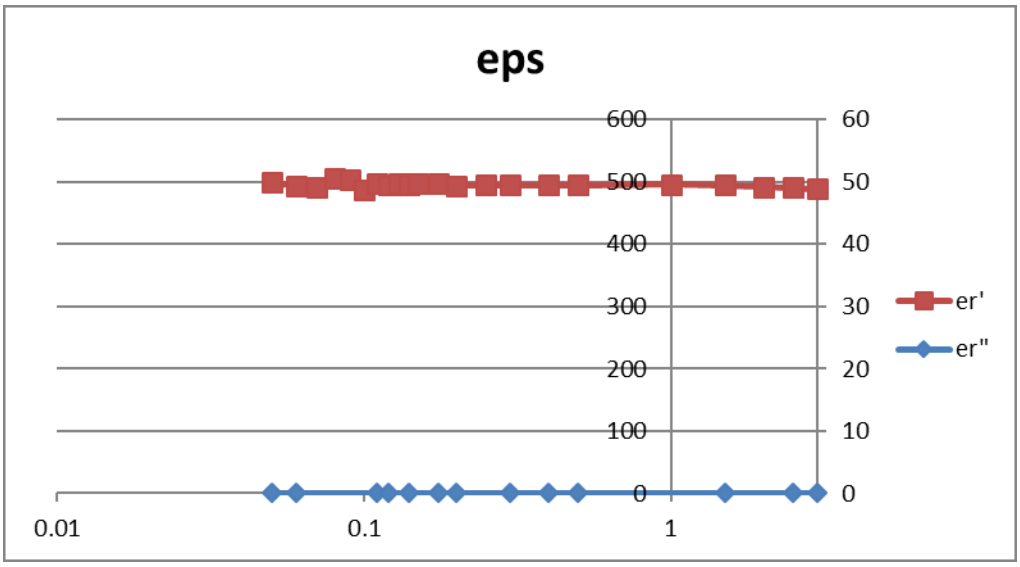

Figure 28: Permittivity measurement of Mn-ferrite thin film

4. INKJET PRINTED PATCH ANTENNA LOADED WITH FERROMAGNETIC METAMATERIAL THIN FILM AND APPLICATION IN ANTENNA MINIATURIZATION

Introduction

One of the challenges hindering the development of a fully inkjet printed and flexible RF front end is the physical dimension of the antenna unit. The performance of an antenna is primarily determined by its size, for e.g. it is a well-known fact that impedance bandwidth of an antenna is directly proportional to the volume of the antenna in wavelengths (Ikonen P. M., 2006). In recent times, developments in microelectronics, light weight, small size and low power requirements of mobile and hand-held devices have increased the demand for small antennas, because of that, antenna miniaturization has experienced a meteoric rise in research interest over the past years, with its attendant challenges due to the limitations of electrically small size antennas. Per (Wheeler H. A., 1947), the antenna size limits efficiency, bandwidth and radiation resistance values. One other limitation of electrically small antenna is the difficulty in correctly feeding the antenna (Staub, O., J-F. Zürcher, and A. Skrivervik., 1998). Therefore, typical antenna design is a compromise between bandwidth, gain, radiation and size. The best compromise is achieved when the entire antenna volume is excited for radiation (Volakis, 2009).

However, different techniques have already been used in literature to achieve antenna miniaturization such as loading the antenna volume with high-contrast materials (Permittivity or permeability), lumped elements, or with conductors using ground planes and short circuits, optimizing the geometry and using the antenna environment (such as radomes and casings) to optimize the radiation (Skrivervik, 2001). One of the common

technique is to load the antenna with high contrast material. Using high dielectric material to achieve antenna miniaturization has been widely explored and reported in literature (Farzami, 2011), (R. K. Mongia, 1994). However, there is a limit to achievable miniaturization as the dielectric's thickness increases. Miniaturization of a printed spiral on the two-different substrate with dielectric values ($^{\varepsilon}_{r} = 9\ and\ 16$) was studied by (Carver, 1981).The miniaturization factor which is a function of thickness, shows a diminishing return after the substrate thickness exceeds 0.1 λ with no observable miniaturization effect after 0.2λ (Volakis, 2009). One major problem associated with high dielectric substrates is that, it enables excitation of surface waves and this leads to low radiation efficiency and high impedance mismatch of the antenna. It also confines most of the excited field in the high permittivity region, leaving only a fraction to be radiated and this reduces the bandwidth of the antenna.

Incorporating a magnetic material on a conventional dielectric substrate introduces an inductive compensation even at microwave frequency and this leads to an efficient size miniaturization of a microstrip antennas. Several antennas incorporating magnetodielectric substrates have been reported in literature (Zhanru, 1999), (Bae, 2005), (Mosallaei, 2007), (Altunyurt, 2009), (Buell, 2006). One of the greatest challenges of a magnetodielectric substrate is that it becomes very lossy at higher frequencies. Per (Hansen R. M., 2000), a dispersion-free substrate with material properties μeff ≫ ɛeff, μeff ≫1, miniaturization of a λ/2 patch antenna shows no adverse effect on the impedance bandwidth. Furthermore, incorporating a magnetic layer on a conventional dielectric substrate improves the radiation quality factor (Q_r) of a λ/2 patch antenna contingent on substrate containing on passive inclusions (Ikonen P. M., 2006). In

addition, to minimize the high loss associated with magnetodielectric substrates at high frequencies, (Erkmen F. C.-C., 2008) used a magnetodielectric layer as a ground plane coating which essentially increases the distance between the printed antenna and the magnetic layer thereby reducing the loss at high frequency due to ferrite layer inclusion. More importantly, the ferrite coating modifies the ground plane reflection coefficient to value between 0 and +1 to enhance conformal antenna radiation even at frequencies when the distance between the antenna and ground plane becomes less than λ/20 (Volakis, 2009).

In this thesis, we present the advantages of magnetic thin film inclusion on a conventional dielectric substrate in antenna miniaturization and performance improvement by comparing the performance characteristics of a λ/2 patch antenna loaded with magnetic metamaterial thin film to that obtained from conventional dielectric substrates, where λ denotes the wavelength in the substrate loaded with magnetic thin film and is related to the free space wavelength λ_0 by $\lambda=\frac{\lambda_0}{\sqrt{\varepsilon_r \mu_r}}$. Rotational measurements of the patch antennas operating at 10GHz, sweeping from 0 to 360 degrees is experimentally demonstrated. Full-wave EM simulation is also performed using HFSS to verify experimental results.

Microstrip Patch Antenna Design

The transmission line model was used in designing the physical dimensions of the patch antenna figure 29a, because these dimensions are finite along the width and length, the fields at the edges of patch exhibit fringing due to the air-substrate interface. The fringing effect makes the patch to look electrically larger than its physical dimension

(Balanis, 2005). To account for the fringing effect, an effective dielectric constant is introduced in the design of the patch antenna.

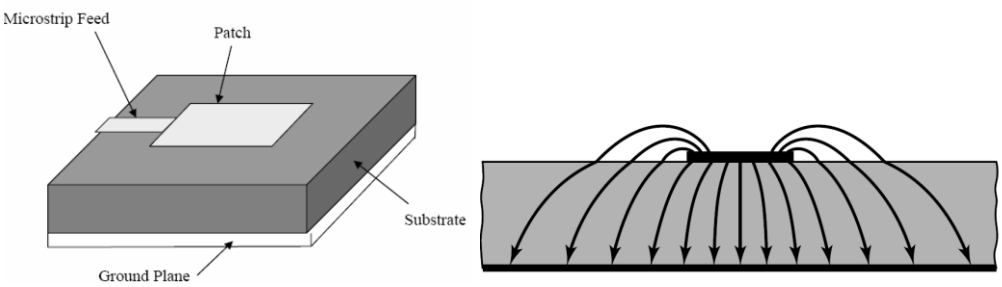

(a) Patch Antenna (b) Electric filed lines

Figure 29: **A Microstrip Patch Antenna and the Electric field distribution**

The width and the length of the patch is made approximately $\lambda_g/2$ (λ_g is the wavelength of the operating RF signal in the substrate). Since the dimension is designed to help maximize efficiency, we use the average of the value for ε_r of the substrate and ε_r of air (=1) to obtain a half-wavelength when we design the width W as shown in equation 4.1.

$$W = \frac{c}{2f_0\sqrt{\frac{\varepsilon_r + 1}{2}}} \tag{4.1}$$

The effective dielectric constant due to the air/dielectric boundary is expressed as ε_{eff} and given by (Balanis, 2005):

$$\varepsilon_{eff} = \frac{\varepsilon_r + 1}{2} + \frac{\varepsilon_r - 1}{2}\left(1 + \frac{10h}{W}\right)^{-1/2} \tag{4.2}$$

Due to the fringing fields along the radiating edges of the antenna there is a line extension ΔL associated with the patch, which is given by (Balanis, 2005):

$$\Delta L = 0.412h\frac{(\varepsilon_{eff}+0.3)(\frac{W}{h}+0.264)}{(\varepsilon_{eff}-0.258)(\frac{W}{h}+0.8)} \quad (4.3)$$

The effective length of the antenna due to the substrate dielectric constant is given by:

$$L_{eff} = \frac{c}{2f_0\sqrt{\varepsilon_{eff}}} \quad (4.4)$$

Therefore, the design length of the microstrip antenna will be the effective length minus the line extension on both edges, which is expressed as

$$L = L_{eff} - 2\Delta L \quad (4.5)$$

In this work, a GaAs wafer with dielectric constant of 12.9 and thickness of 625um was used, the dimensions of the 10GHz patch antenna were calculated as W = 5.689mm, L = 4.04mm, where W is the width and L is the Length of the antenna.

Fabrication and Measurement

Test samples were fabricated under normal laboratory conditions. Two different categories of samples were prepared for this study, one category has a ferrite thin film in between the substrate and the antenna while the second category has no ferrite thin film layer as shown in figure 4.2. On one of the samples, a 2cmX2cm square ferrite thin film was printed on GaAs substrate with thickness of 625micron and microwave dielectric constant of 12.9, using Fujifilm Dimatix Materials inkjet Printer (DMP-2800). For optimum deposition of the ferromagnetic ink, the print-head of the inkjet printer was adjusted to print the ferrite ink in 25µm drop spacing at a resolution of 360 x 360 dpi (dots per inch), the jetting frequency is maintained at 7 kHz and the platen temperature was kept at 50˚C with a maximum nozzle voltage of 30V. After printing the ferrite film,

the sample was sintered for 15 minutes on a hot plate at 120˚C. The surface morphology and profile of the ferrite thin film were both measured using Park SYSTEMS XE7 Atomic Force Microscope and KLA Tencor P-7 Profilometer respectively. A nano-silver ink (Novacentric ink) was used to print a 4.04mm X 5.69mm microstrip patch antenna on top of the ferrite film. The printing procedure for the patch antenna printing is the same for the ferrite film except that the drop spacing was increased to 50µm. The sintering of the nano-silver ink involved curing the sample on a hot plate for an initial low temperature of 100˚C for 10 minutes and thereafter, the temperature was increased to 220˚C for 20 minutes.

The second category of samples were fabricated by printing only the patch antenna on the substrate following the same procedure as above.

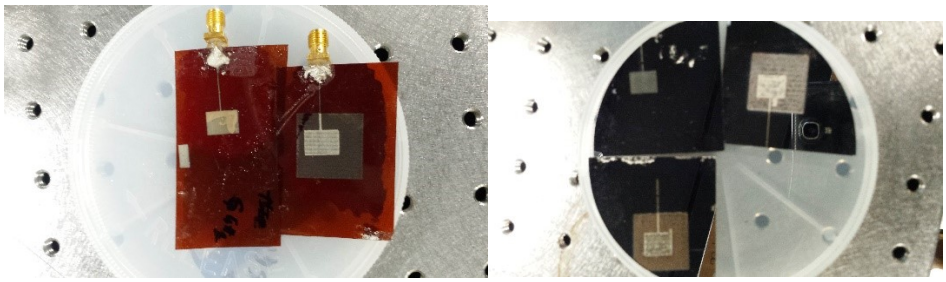

(a) Kepton (b) GaAs

Figure 30: **Test samples showing the two different categories of patch antenna on a ferrite thin film and without a ferrite thin film on (a) kepton substrate and (b) GaAs wafer.**

The S11 measurement for the different samples was carried out using Agilent Vector Network Analyzer (VNA), across the frequency range of 50MHz to 13.5GHz. The VNA was connected to a Newport 271 probe station with 40A-SG-500-C GSG probes

shown in figure 31. To ensure the validity of our results, a system calibration was performed to remove all systematic errors. An Open-Short-Load- Through (OSLT) full two port calibration was performed to set the reference planes at the tip of the probes. Thereafter, an SMA connector was connected to the microstrip line to verify the repeatability of our measurement and result. We created a test setup as shown in figure 32, to measure the far-field characteristics and also test the beam steering of our antenna. The setup was automated to eliminate personnel involvement in data collection.

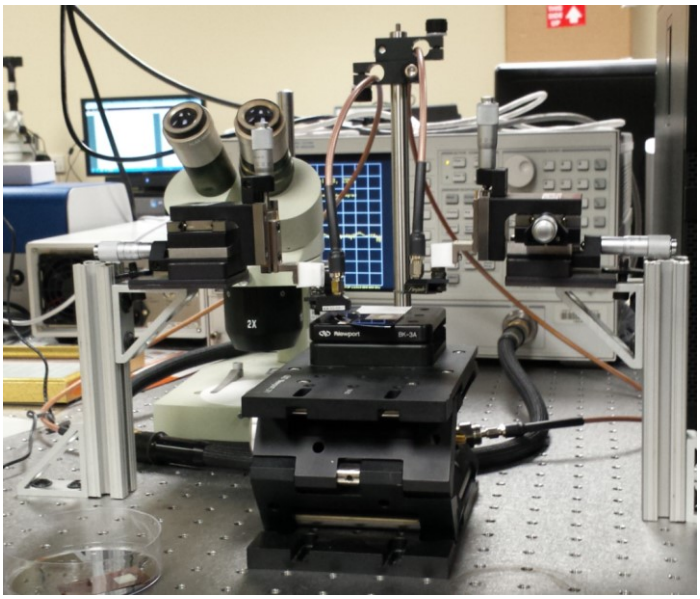

Figure 31: **VNA probe station for S11 measurement**.

The measurement setup consists of a microwave spectrum analyzer connected to a horn antenna, a signal generator, a rotational stage with a stepper motor that enables 2 degrees of freedom and controlled by an Arduno microcontroller, a Pyhthon programing language was used to develop a computer program that controls the whole setup. In taking measurements, the stage moves to the set position, a signal generator generates signal at a specific frequency which is sent to the antenna under test (AUT), the received signal

power by the horn antenna connected to the spectrum analyzer is recorded and the computer automatically plots the far-field radiation pattern of the AUT.

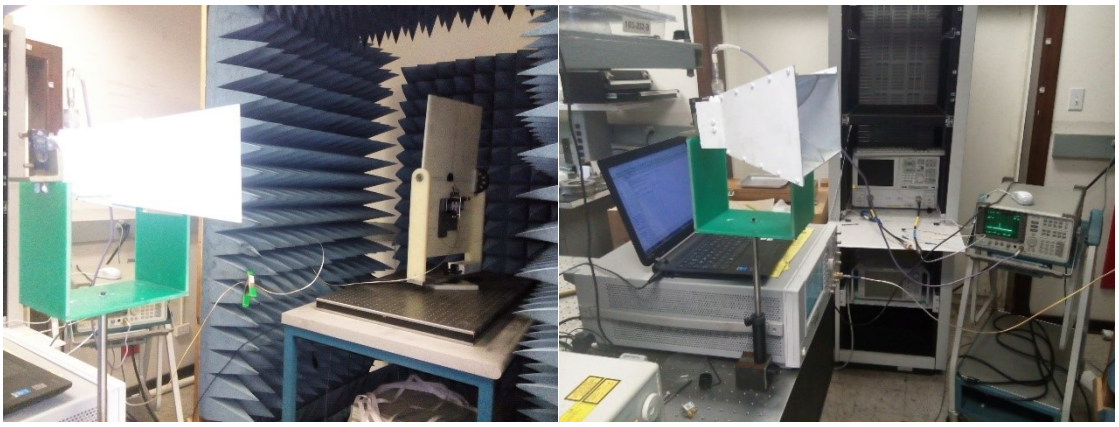

Figure 32: Antenna Far-field measurement setup

Results and Discussion

The two categories of the antenna samples were measured and compared in antenna performance. The measurement results were also compared to the simulation results. To ensure good antenna performance, a good quality ferrite thin film layer devoid of defect is desirable. The relative permeability (μ_r=6) of the film was measured using microstrip transmission line permeameter. The Complete characterization of the ferrite thin film is discussed in (Enuka, 2017). Figures 33 and 34 shows the profilometer measurement of 5um and 10um thick ferrite film deposited on GaAs using inkjet printing. The average roughness of the thin films as measured are 0.012um and 0.438um respectively while the average waviness is 0.01um and 0.68um respectively. These values show that the surface profile of the ferrite film is relatively smooth. This is important

because it helps to avoid nucleation sites that might lead to cracking and degradation of the antenna performance.

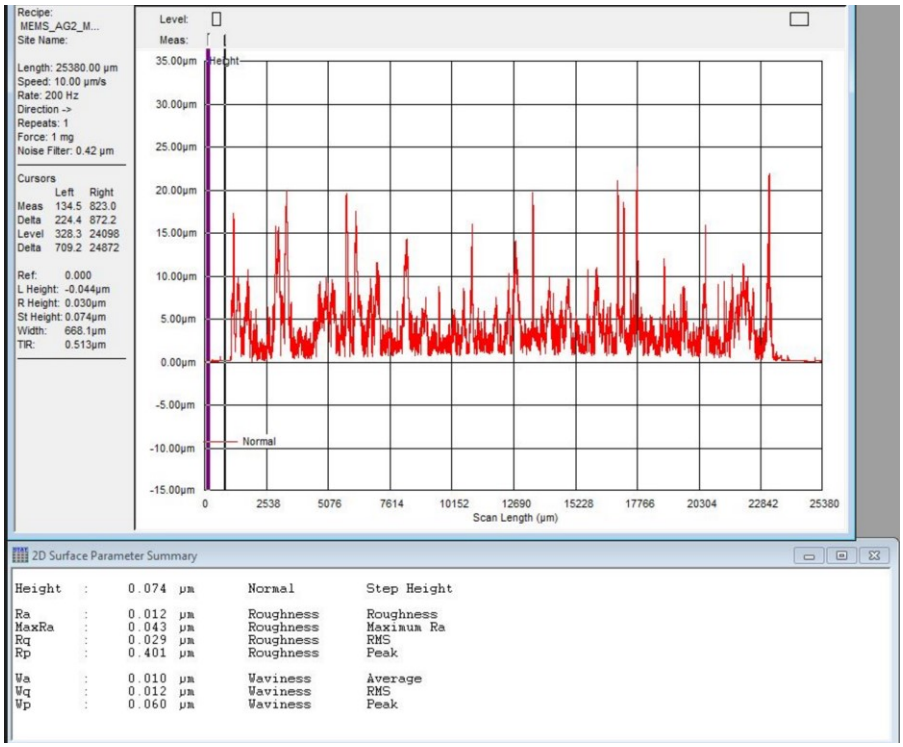

Figure 33: **5um thick ferrite film**

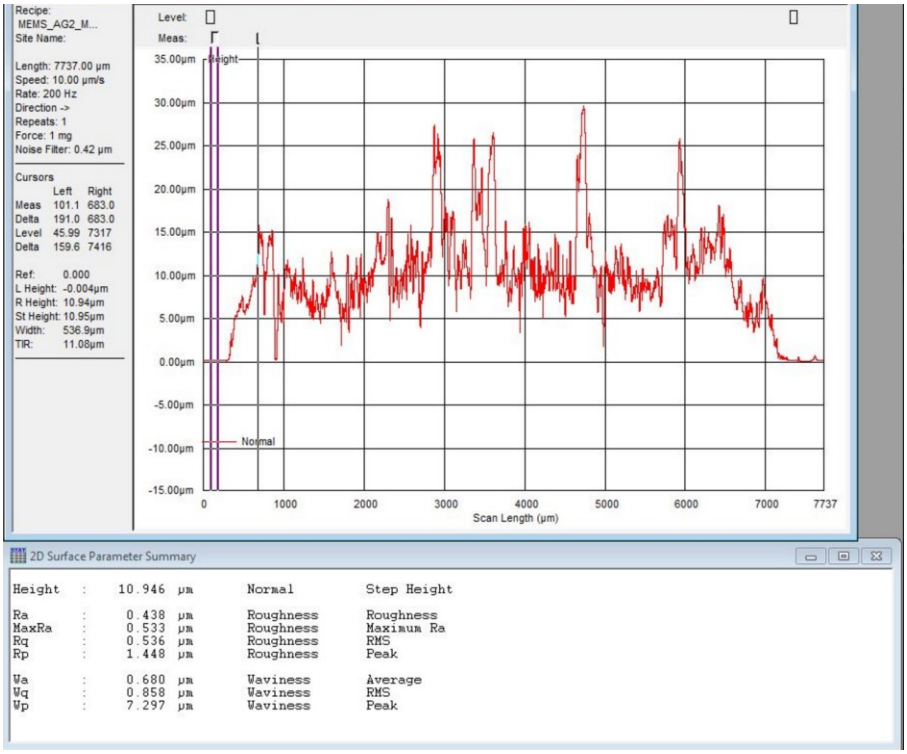

Figures 34: **10um thick ferrite film**

Hfss was used to simulate the microstrip patch antennas on dielectric and magnetodielectric substrates. The simulation designs are shown below.

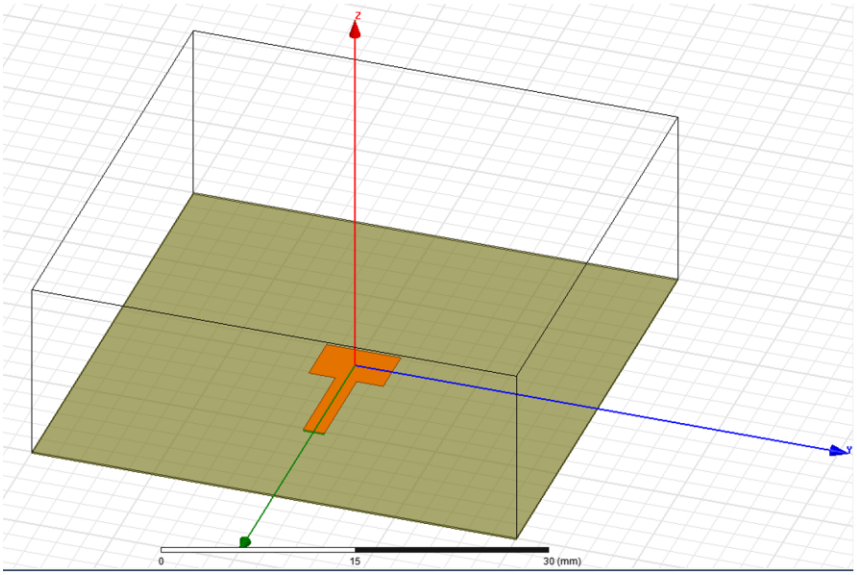

Figure 35: MPA on dielectric substrate

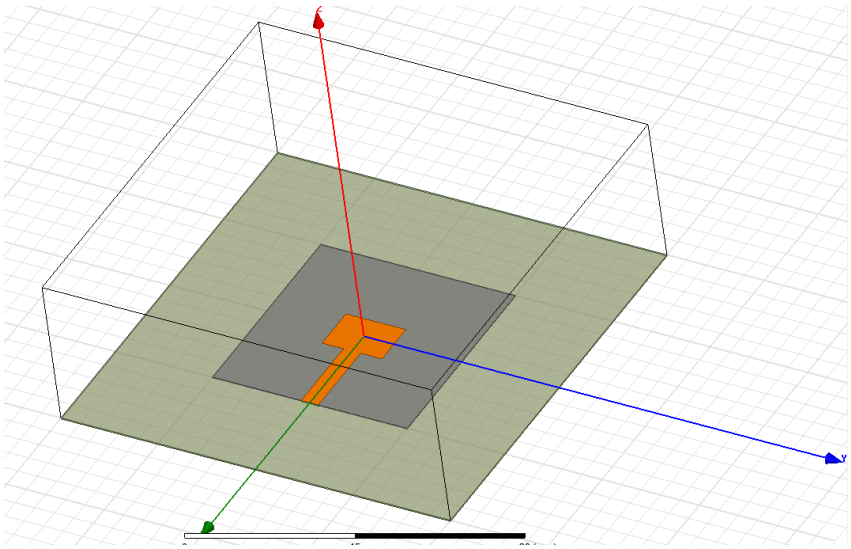

Figure 36: MPA on magnetodielectric substrate

The radiation characteristics of the antenna on dielectric substrate was simulated and the compared the experimental measured data. The gain of the antenna on dielectric substrate is about 5.5dB.

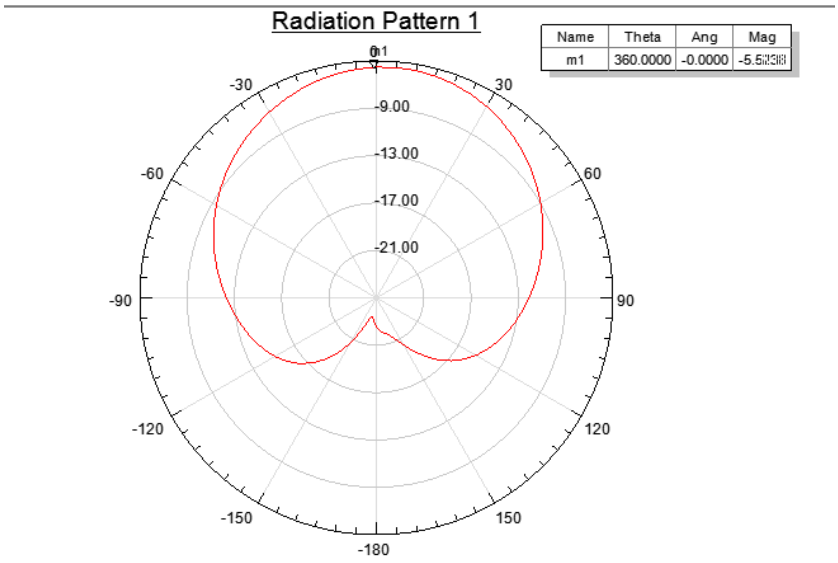

Figure 37: Radiation Pattern of the antenna on dielectric substrate.

A return-loss of less than -10dB is used to determine the radiation and bandwidth of the antenna. As shown in figure 4.10, the resonance frequency of the patch antenna without magnetic inclusion is 9.7GHz. The frequency is reduced to 8.7GHz when the antenna is printed on ferrite thin film of 5um thickness. The reduction in resonance frequency is due to the magnetic inclusion. When the thickness of the ferrite film is increased to 10um, the resonance frequency is further reduced to about 5.9GHz. However, it was observed that the bandwidth of the antenna began to decrease after a certain critical thickness due to increased loss associated with the ferrite at high frequencies and also increase in thickness caused more of the electric field to be confined in high dielectric region introduced by the ferrite layer. In addition to the magnetic effect of the ferrite film, as the thickness of the ferrite film increases, the distance between the patch and ground plane also increases and the effective current path of the antenna is increased, thus leading to more reduction in resonance frequency.

The measured radiation patterns of the antenna at its resonance in the elevation-cut plane (phi = 0°) normalized to the simulated radiation pattern is shown in figure 40. The gain of the antenna on a dielectric (without ferrite film) substrate is about 13dBi while a gain of 17dBi is obtained with the magnetic ferrite inclusion. The half power beamwidth (HPBW) of the antenna on a magneto-dielectric substrate is 140˙ while on the dielectric substrate, it is 103˙.

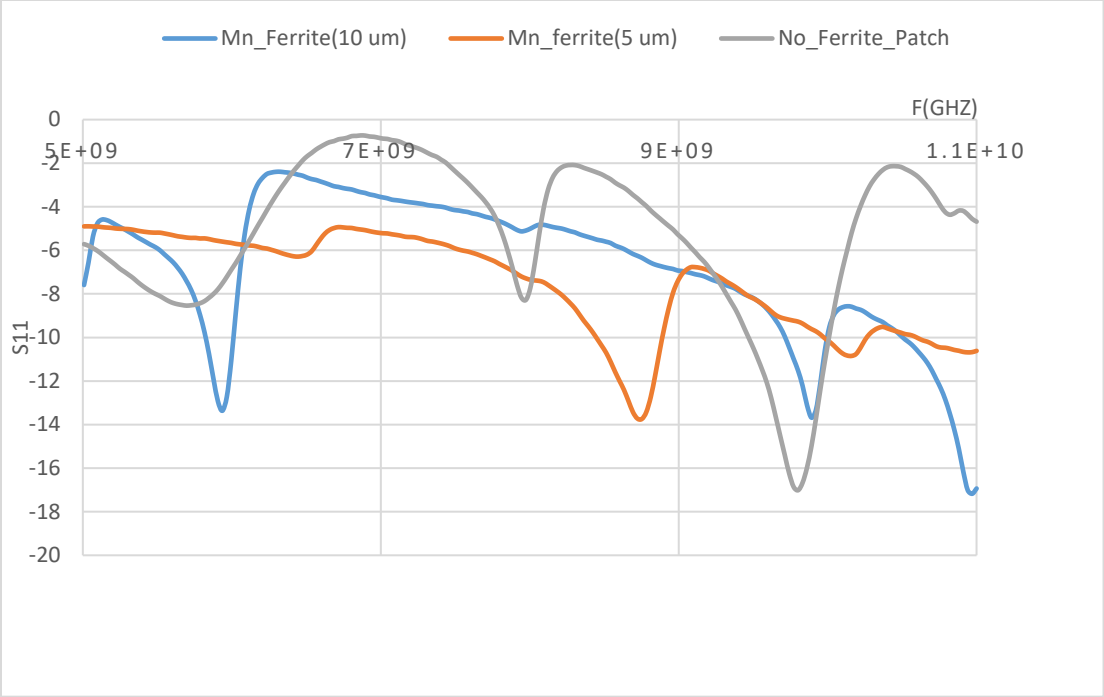

Figure 38: **Return loss measurement of the Magneto-dielectric and dielectric substrate**

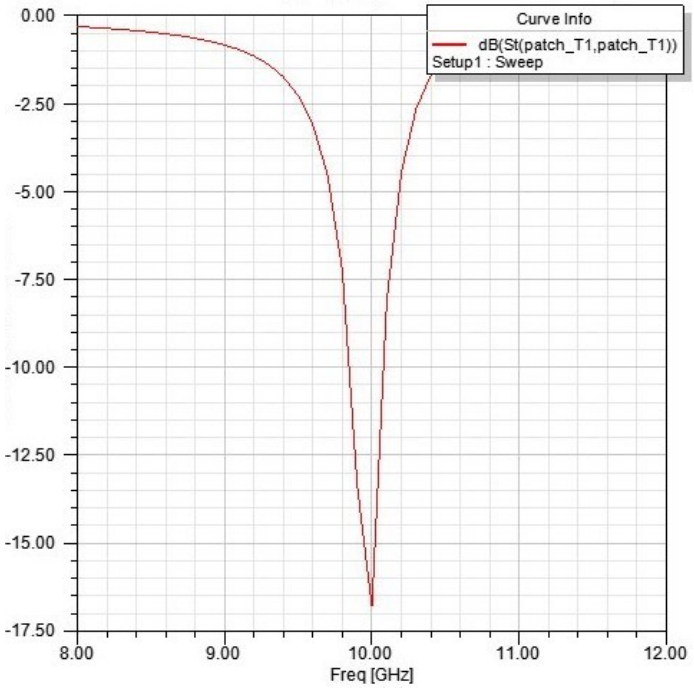

Figure 39: **Return loss simulation of the patch antenna**

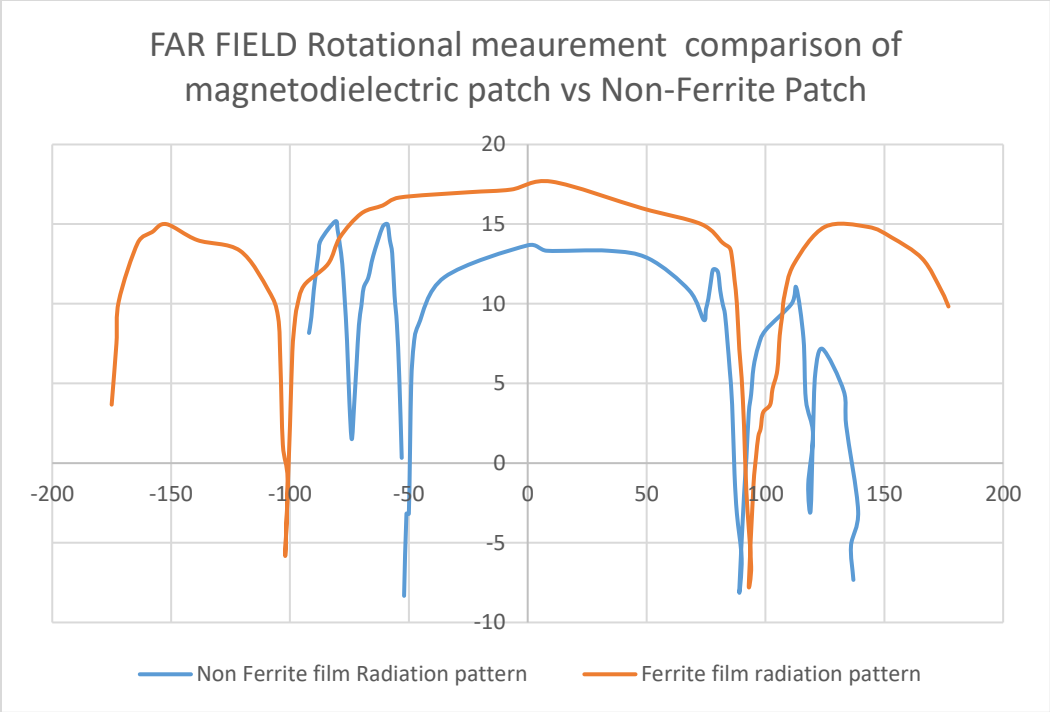

Figure 40: **Radiation pattern measurement of the Magneto-dielectric and dielectric only substrate**

5. CONCLUSION AND RECCOMENDATIONS FOR FUTURE WORK.

Introduction

The current trend in communication and electronic device manufacturing industry is towards small size mobile gadgets. There is large development and usage of mobile phones, tablets, computers, laptops, GPS navigators etc, which are connected with wireless access points to exchange and transfer data or information. Furthermore, the demand for hand held commercial and military mobile wireless devices have pushed for more size reduction of electronic devices. Wireless systems and their size reduction has become a very important issue in recent time.

One of the challenges hindering the development of a fully inkjet printed and flexible RF front end is the physical dimension of the antenna unit. It is a well-known fact that the key performance parameters of an antenna e.g. bandwidth, radiation efficiency, gain etc. are tightly dependent upon the physical dimensions of the structure. In order to establish standing

electromagnetic waves, the dimension of the resonant structure needs to be at least half a wavelength, which imposes a size limitation. The aforementioned issues have so far precluded integration of antennas monolithically into the rest of the transceiver circuitry. As a result of this, efficient antenna miniaturization technique has become imperative.

In a bid to provide solution to the aforementioned problems, the objective of this thesis was to provide a novel miniaturization technique for planar antennas.

Contributions

The contributions of this thesis can be summarized via

Development of ferromagnetic ink suitable for inkjet printer

Inkjet printing technique, being an additive deposition technique has become a preferred device fabrication choice compared to contemporary lithographic method. It enables drop-on-demand, which is very important for material conservation and low cost of fabrication. Since it was observed that magnetic inclusion on conventional dielectric substrates helps to overcome the inherent limitations on the performance of an antenna fabricated on dielectric substrates such as narrow bandwidth and radiation loss, magnetodielectric substrates has witnessed a tremendous increase in research interest. Different deposition techniques such as sputtering, PLD, Spin coating have been used to achieve magnetodielectric substrate.

However, because of the challenges in dispersing ferromagnetic particles in a liquid medium due to average size and weight of the particles, agglomeration of particles, there is no commercially available ferromagnetic ink suitable for inkjet printing and therefore it becomes more challenging to achieve magnetodielectric substrates using inkjet printing technique. This thesis provided a solution to this problem by disclosing a novel method of developing a low curing temperature, ferromagnetic ink suitable for inkjet printing. The feasibility in inkjet printing technology was demonstrated by printing a Nickle-Zinc ferrite and Manganese ferrite film using inks prepared by this method. Chapter three summarizes the method and characterization of the ferrite thin films thereof. The results obtained from the characterization shows that the films possess properties required for microwave frequency application such as high resistivity etc. The constitutive parameters of these films also reveal their stability at microwave frequency range. The comparison between the thin film and bulk material is also summarized in chapter three.

Antenna Miniaturization

Antenna miniaturization as a field of research has experienced a meteoric rise in research interest as result of increasing demands for small size antennas. The dependency of antenna performance parameters on the physical dimensions of the antenna element was discussed in chapter one. Limitations of electrically small antenna was extensively discussed too. In this thesis, a method for reducing the size of an antenna without compromising its performance was shown. The method employs magnetodielectric substrate and was demonstrated using microstrip patch antenna. We compared the performance characteristics of a λ/2 patch antenna loaded with magnetic metamaterial thin film to that obtained from conventional dielectric substrates. Rotational measurements of the patch antennas operating at 10GHz from 0 to 360 degrees is experimentally demonstrated. Full-wave EM simulation is also performed using HFSS to verify experimental results. The antenna on magnetodielectric substrate showed a significant size reduction with improved performance. The simulation and measurement results were discussed in chapter four. The limitation on the thickness of the ferrite thin film was also highlighted.

Recommendations for future work

As a result of the importance of miniaturized antennas in wide variety of applications, we hope to extend this research by

1. Developing a fully magnetic biosensor incorporating a miniaturized antenna to monitor both body temperature and pulse rate,
2. Developing a magnetic transistor with an improved ON/OFF ratio.

REFERENCES

Altunyurt, N. e. (2009). Antenna miniaturization using magneto-dielectric substrates. *59th Electronic Components and Technology Conference*.

Bae, S. a. (2005). A small meander VHF & UHF antenna by magneto-dielectric materials. *Asia-Pacific Microwave Conference Proceedings. Vol. 4.*

Balanis, C. A. (2005). *Antenna Theory, Analyysis and design.* San Marcos: JOHN WILEY & SONS, INC.,.

Buell, K. H. (2006). A substrate for small patch antennas providing tunable miniaturization factors." (): . *IEEE Transactions on Microwave Theory and Techniques 54.1*, 135-146.

Burke, H. R. (2000). Antenna with magneto-dielectrics. *Microwave Opt. Technol. Lett., vol. 26, no. 2*, 75-78.

Carver, K. a. (1981). Microstrip antenna technology. *IEEE transactions on antennas and propagation 29.1*, 2-24.

Carver, K. a. (1981). Microstrip antenna technology. *IEEE transactions on antennas and propagation 29.1*, 2-24.

Cheon Y., L. J. (2012). Quad-band monopole antenna including LTE 700 MHz with magneto-dielectric material. *IEEE Antennas Wireless Propag. Lett., vol. 11*, 137-140.

Chi, P. L. (2011). Antenna miniaturization using slow wave enhancement factor from loaded transmission line models. *IEEE Transactions on Antennas and Propagation, 59(1)*, 48-57.

Chu, L. J. (1948). Physical limitations on omni-directional antennas. *J. Appl.Phys., vol. 19*, 1163-1175.

Colburn, J. S.-S. (1999). Patch antennas on externally perforated high dielectric constant substrates. *IEEE Transactions on Antennas and Propagation, 47(12)*, 1785-1794 .

Daliya S. Mathew, R.-S. J. (2007). An overview of the structure and magnetism of spinel ferrite nanoparticles and their synthesis in microemulsions. *Chemical Engineering Journal Volume 129, Issues 1–3*, 51–65.

Dionne, G. F. (2003). Magnetic relaxation and anisotropy effects on high-frequency permeability. *IEEE transactions on magnetics, 39(5)*, 3121-3126.

Enuka, E. X. (2017). Method of preparing a polar based magnetic ink suitable for inkjet printing and characterization of Ni and Mn ferrite thin film. *Advances in Functional Materials.*

Erkmen, F. C. (2008). . UWB magneto-dielectric ground plane for low-profile antenna applications. . *IEEE Antennas and Propagation Magazine, 50(4).*

Erkmen, F. C.-C. (2008). UWB magneto-dielectric ground plane for low-profile antenna applications. *IEEE Antennas and Propagation Magazine 50.4* , 211-216.

Farzami, F. K. (2011). Miniaturization of a microstrip antenna using a compact and thin magneto-dielectric substrate. *EEE Antennas and Wireless Propagation Letters 10* , 1540-1542.

Gorkunov M. Lapine M., S. a. (2002). Effective magnetic properties of a composite material with circular conductive elements. *Eur. Phys. J. B, vol. 28, no. 3*, 263–269.

Gustafsson M., S. C. (2007). Physical limitations on antennas of arbitrary shape. *Proceedings of Royal society A: Mathematical, Physical and Engineering sciences, vol. 463*, (pp. 2589-2607).

Han, K. H. (2015). *magneto-dielectric material characterization.*

Hansen, R. C. (1981). Fundamental limitations in antennas. *Proc. ZEEE, vol. 69*, (pp. 170-182).

Hansen, R. M. (2000). Antennas with Magneto-Dielectrics. *Microwave and Optical Technology Letters, vol. 26, no. 2*, 75-78,.

Harrington, R. F. (1960). Effect of antenna size on gain, bandwidth and efficiency. *J. Res. Nut. Bur. Stund., vol. 64-D*, 1-12.

Hossein M, a. K. (2004). Magneto-Dielectrics in Electromagnetics: Concept and Applications. *IEEE TRANSACTIONS ON ANTENNAS AND PROPAGATION, VOL. 52, NO. 6,*, (pp. 1558-1567).

Huynh M.C., S. W. (2004). Ground plane effects on planar inverted F antenna (PIFA) performance . *IEEE Procedings Microwave, Antennas and Propagation vol.50*, 27-29.

Hwang Y., Z. Y. (1995). Planar inverted F antenna loaded with permittivity material . *Electronics letter vol.31*, 1710-1711.

Ikonen, P. M. (2006). Magnetodielectric substrates in antenna miniaturization: Potential and limitations. *IEEE Transactions on Antennas and Propagation 54.11*, 3391-3399.

Ikonen, P. M. (2006). On artificial magneto-dielectric loading for improving the impedance bandwidth properties of microstrip antennas," .

http://arxiv.org/abs/physics/0509139. (Accepted in IEEE Trans. Antennas Propagat., .

James S. McLean, M. (1996). A Re-Examination of the Fundamental Limits on the Radiation Q of Electrically Small Antennas. *IEEE TRANSACTIONS ON ANTENNAS AND PROPAGATION, VOL. 44, NO. 5*, 672-676.

Kramer, B. A., Chen, C.-C., & Volakis, J. L. (2008). Size Reduction of a Low-Profile Spiral Antenna Using Inductive and Dielectric Loading. *IEEE Antennas and Wireless Propagation Letters. vol.7*, 22-25.

Last Name, F. M. (Year). *Book Title.* City Name: Publisher Name.

Lee, J. M. (2012). , "Miniaturized antennas with reduced hand effects with magneto-dielectric material. *IEEE Antennas Wireless Propag. Lett., vol. 11*, 137-140,.

Lee, M. K. (2007). Distributed lumped loads and lossy transmission line model for wideband spiral antenna miniaturization and characterization. . *IEEE Transactions on Antennas and Propagation, 55(10)*, 2671-2678.

Lo T.K., H. J. (2004). Small wideband PIFA for mobile phones at 1800MHz. *Vehicular Technology conference*, (pp. 27-29).

Mahmoud Goodarz Naseri, E. B. (2012). *Crystalization in Spinel Ferrite Nanoparticles.* Universiti Putra Malaysia.

Mak, K. M., Lai, H. W., Luk, K. M., & Chan, C. H. (2014). Circularly Polarized Patch Antenna for Future 5G Mobile Phones. *IEEE Access. vol.2* , 1521-1529.

Marqués, R. M.-E.-I. (2002). Role of bianisotropy in negative permeability and left-handed metamaterials. *Phys. Rev. B, vol. 65, no. -6*, 1444401.

McElligott, M. a. (2004). *Process for the preparation of aqueous magnetic ink character recognition ink-jet ink compositions.* Google Patents.

Mosallaei, H. a. (2007). Design and modeling of patch antenna printed on magneto-dielectric embedded-circuit metasubstrate." (): . *IEEE transactions on antennas and propagation 55.1*, 45-52.

Néel L. (1948). Propriétées magnétiques des ferrites; Férrimagnétisme et antiferromagnétisme. *Annales de Physique (Paris) 3,*, 137-198.

Paul, B. M. (1997). Microemulsions: an overview. *J. Dispers. Sci. Technol., 18* , 301–367.

R. K. Mongia, A. I. (1994). Low profile dielectric resonator antennas using a very high permittivity material. *Electron Lett., vol. 30, no. 17*, 1362–1363.

Rashed J., T. C. (1982). A new class of wire antennas. *IEEE Antennas and propagation society international symposium, vol.20*, 564-567.

Scardelletti, M. C. (2008). Electrically small folded slot antenna utilizing capacitive loaded slot lines. *Radio and Wireless Symposium*, 731-734.

Shin, Y. S. (2010.). A monopole antenna with a magneto-dielectric material and its MIMO application for 700 MHz-LTE-band," . *Microw. Optical Technol. Lett., vol52, no. 10*, 2364-2367.

Skrivervik, A. K. (2001). PCS antenna design: The challenge of miniaturization. *IEEE Antennas and Propagation Magazine 43.4*, 12-27.

Sorensen K.J., K. C. (2001). *Nanoscale Materials in Chemistry.* Wiley, New York .

Stanciu, D. A. (2006). Ultrafast spin dynamics across compensation points in ferrimagnetic GdFeCo: The role of angular momentum compensation. *Phys. Rev. B 73, 220402(R)*.

Staub, O., J-F. Zürcher, and A. Skrivervik. (1998). Some considerations on the correct measurement of the gain and bandwidth of electrically small antennas. *Microwave and Optical Technology Letters 17.3*, 156-160.

Thal H.L. (2006). New Radiation Q limits for spherical wire antennas. *IEEE transactions on antennas and propagation vol AP-54*, 1879-1885.

Thiele G.A., D. P. (2003). On the lower bound of the radiation Q for electriccally small antennas . *IEEE Transactions on Antenna and Propagation, vol AP-51* , (pp. 1263-1269).

Vestal, C. Z. (2004). Magnetic spinel ferrite nanoparticles from microemulsions. *Int. J. Nanotechnol., 1* , 240–263.

Volakis, J. C.-C. (2009). *Small antennas: miniaturization techniques & applications.* McGraw Hill Professional.

Wang, Y. C. (2004). High-coercivity Co-ferrite thin films on (100)-SiO 2 substrate. *Applied Physics Letters, 84(14)*, 2596-2598.

Waterhouse R. B., T. S. (1998). Design and performance of small printed antennas. *IEEE transactions on antennas and Propagation. vol.46*, 1629-1633.

Wheeler, H. A. (1947). Fundamental limitations of small antennas. *Proceedings of the IRE 35.12*, (pp. 1479-1484.).

Wheeler, H. A. (1947). Fundmental limitations of small antennas. *Proc. IRE,vol. 35*, (pp. 1479-1484).

Wheeler, H. A. (1975, July). Small antennas. *IEEE Trans. Antennas Propagat., vol. AP-23,* , pp. 462-1169.

Youngs, I. J. (2005). Dielectric relaxation in metal-coated particles: the dramatic role of nano-scale coatings. *J. Phys. D: Appl. Phys., vol. 38, pp. ,* , 188-201.

Zhanru, L. a. (1999). New type organic magnetic materials and their application in the field of microwaves. *Journal of Microwares 4* .

Zhou Y. Chen C. C., V. J. (2009). A compact 4 element dual band GPS array. *IEEE Antennas and Propagation Society International Symposium, vol. 1-5*, 1-4.

Ziolkowski, Y. S. (2003). Bandwidth of a microstrip patch antenna on a magneto-dielectric substrate. *IEEE Antennas Propagat. Soc. Int. Symp*, (pp. 297–300.). Columbus, OH.